Accepted Manuscript

Journal of the Geological Society

Magmatic arc evolution during the tectonic closure of the Rocas Verdes basin: insights from Cretaceous-earliest Paleocene intrusive rocks of Navarino Island (55°S), Fuegian Andes

Ricardo Velásquez, Joaquín Bastías, Esteban Salazar, Fernando Poblete, Mauricio González Guillot, David Chew, Matías Peña, Felipe Tapia, Adán Ramirez & Foteini Drakou

DOI: https://doi.org/10.1144/jgs2022-163

To access the most recent version of this article, please click the DOI URL in the line above. When citing this article please include the above DOI.

Received 22 November 2022
Revised 26 May 2023
Accepted 31 May 2023

Supplementary material at https://doi.org/10.6084/m9.figshare.c.6675416

Magmatic arc evolution during the tectonic closure of the Rocas Verdes basin: insights from Cretaceous-earliest Paleocene intrusive rocks of Navarino Island (55°S), Fuegian Andes

Ricardo Velásquez[a*], Joaquín Bastías[b,c], Esteban Salazar[a], Fernando Poblete[d,e], Mauricio González Guillot[f,g], David Chew[b], Matías Peña[h], Felipe Tapia[i], Adán Ramirez[j], Foteini Drakou[b]

[a] Servicio Nacional de Geología y Minería, Avenida Santa María 0104, Providencia, Santiago, Chile
[b] Department of Geology, School of Natural Sciences, Trinity College Dublin, College Green, Dublin 2, Ireland
[c] Carrera Geología, Facultad de Ingeniería, Universidad Andres Bello, Chile
[d] Universidad de Chile, Departamento de Geología, Plaza Ercilla 803, 8370450 Santiago, Chile
[e] Universidad de O'Higgins, Instituto de Ciencias de la Ingeniería, Rancagua, Chile
[f] Centro Austral de Investigaciones Científicas (CADIC-CONICET), Houssay 200, Ushuaia, Argentina
[g] Instituto de Ciencias Polares, Ambiente y Recursos Naturales, UNTDF, Fuegia Basket 251, Ushuaia, Argentina
[h] Escuela de Geología, Universidad Mayor, Manuel Montt 367, Providencia, Santiago, Chile
[i] Facultad de Ciencias Exactas y Naturales, Departamento de Ciencias Geológicas, Universidad de Buenos Aires. Consejo Nacional de Investigaciones Científicas y Técnicas, Instituto de Estudios Andinos "Don Pablo Groeber" (IDEAN)
[j] Servicio Nacional de Geología y Minería, Til Til 1993, Ñuñoa, Santiago, Chile
* Corresponding author

Abstract

Navarino Island is located in the southernmost part of the Fuegian Andes, south of the Beagle Channel. It geological record documents the complex tectonic history of Tierra del Fuego that includes the opening and closure of the Rocas Verdes basin, Cordillera arc collision and subsequent subduction processes. The geology of the island is mostly comprised of the Cretaceous Yahgán Formation, a marine meta-sedimentary sequence, which is intruded by diverse plutons that are mostly exposed on the northwestern tip of the island. We herein present a new dataset that shows the presence of three Cretaceous-earliest Paleocene magmatic suites of active margin magmatism emplaced during the early stage of the Fuegian Andes, which are referred to as (i) the Dientes de Navarino Microdioritic Sills, a suite of pre-tectonic microdioritic sills that formed during ~101-97 Ma; (ii) the Castores Plutonic Complex, a series of pre- to syn-tectonic gabbroic to tonalitic plutons emplaced during ~90-87 Ma and (iii) the Samantha Monzonites, a suite of isolated monzonitic to monzodioritic post-tectonic plutons that formed at ~66-65 Ma. These distinct magmatic episodes are recognised by field observations, geological mapping, petrography and whole-rock geochemistry integrated with amphibole and biotite

$^{40}Ar/^{39}Ar$ and U-Pb zircon LA-ICP-MS geochronology. The geochemical compositions of these rocks are consistent with a continental arc setting that formed during the interval ~101-65 Ma. While the three pulses spatially overlap in Navarino Island, the arc magmatism shows a migration (or expansion) throughout the Late Cretaceous. The locus of the arc then migrates at ~68-66 Ma towards the southwest. We suggest that this trench-ward migration at ~68-66 Ma may be associated with a change in the subduction angle. The three Cretaceous- earliest Paleocene plutonic pulses recorded in Navarino Island formed during the early stages of development of the Fuegian Andes, and are pre-, syn-and post-tectonic with respect to a major compressional event caused by the collision and obduction of the back-arc Rocas Verdes oceanic floor.

Keywords: Fuegian Andes, Patagonia, Cretaceous, magmatism, Rocas Verdes.

1. Introduction

Magmatism on convergent plate margins is often intimately associated with the development of orogenic belts. Located at the southern tip of the Fuegian Andes, Navarino Island exceptionally preserves different stages of magmatism during the Cretaceous–earliest Paleocene.

While there have been different studies shedding light on the geological units (Kranck, 1932; Katz and Watters, 1966; Suárez *et al*., 1985; Salazar *et al.*, 2021), stratigraphy (Suárez *et al*., 1985) and magmatic bodies (Suárez *et al*., 1982, 1985, 1987) of Navarino Island, we still lack a thorough geochronological and geochemical framework for the intrusive rock suites. Furthermore, their temporal constraints, emplacement style and general petrology remains relatively unknown, along with their relationship or significance to the major tectonic events in the region, such as the closure and inversion of the Rocas Verdes marginal basin. Therefore, these units have significant potential to yield important information to better understand the tectonic and magmatic evolution of the early stages of the Fuegian Andes

The intrusive rocks of southernmost South America (south of 53°S) have been grouped in the Fuegian Batholith (Hervé *et al*., 2007) and the Fuegian Potassic Magmatism (Gonzalez-Guillot *et al*., 2009), which are both part of the Fuegian Andes. While the Fuegian Batholith corresponds to a group of calc-alkaline plutons that formed from the Late Jurassic until the Paleocene (Hervé *et al*., 1984; Suárez *et al*., 1985; Poblete *et al*., 2016), the Fuegian Potassic Magmatism corresponds to small suite of isolated, shoshonitic plutons exposed in the southeast of Tierra del Fuego Island, north of the Beagle Channel, in a rear-arc position (Fig. 1; González Guillot *et al*., 2009; González Guillot, 2016). The batholith developed during and after the opening and closure of the Rocas Verdes basin, which is a back-arc basin that eventually developed oceanic lithosphere during the Late Jurassic- Early Cretaceous (Stern and de Wit, 2003; Klepeis *et al*., 2010).

Navarino Island is located to the south of the Beagle Channel (Fig. 1). Its exposures are dominated by the marine meta-sedimentary rocks of the Cretaceous Yahgán Formation (Kranck, 1932; Suárez *et al*., 1985). Also exposed is the Tortuga Ophiolitic Complex in the southernmost part of the island, along with Late Cretaceous-earliest Paleocene plutons. These plutons are part of the I-type calc-alkaline Fuegian Batholith. This study contributes new geochronological data (zircon U-Pb LA-ICP-MS and amphibole and biotite $^{40}Ar/^{39}Ar$ dating), field observations, petrography and major and trace element whole-rock geochemistry of the main Cretaceous-earliest Palaeocene igneous units of Navarino Island. These results are integrated into a detailed geochronological and geochemical characterisation of these units, which contributes to a better understanding of the magmatic evolution of the Fuegian Batholith and its associated units such as the rear-arc magmatic bodies. Additionally, it helps our understanding of how the margin evolved within the context of the collision between the arc and the continent during closure and inversion of the Rocas Verdes basin. In combination, this allows correlation with other contemporaneous plutonic units in the region and shows that these rocks formed within an active margin setting from ~101 to 65 Ma.

2. Geological setting

The Patagonian Batholith continuously extends along the continental margin between 56-40°S (Hervé *et al*., 2007). It is divided into three major segments: the North Patagonian Batholith (north of 47°S), South Patagonian Batholith (53-47°S) and the Fuegian Batholith (south of 53°S). The latter is characterised by multiple magmatic pulses (*e.g*. Montes, 2013), which formed during the Jurassic and continued without interruption until the Palaeocene (Hervé *et al*., 1984). Jurassic magmatism is mostly comprised of plutons that were generated in an active margin setting that experienced extension linked to the breakup of Gondwana and influenced by thermal input from the migrating Karoo mantle plume (Pankhurst *et al*. 2000, Dalziel *et al*. 2013, Navarrete *et al*., 2019), resulting in silicic, mafic and bimodal magmatism (*e.g*., Bruhn *et al*., 1978; Pankhurst *et al*., 2000; Calderón *et al*., 2007). However, it has been recently suggested thatthe Jurassic magmatism of Patagonia was mostly generated from subduction-derived melts (Bastias *et al*., 2021a, 2021b). The related felsic volcanic products (Tobífera Formation) have been recognised northeast of the Fuegian Batholith with U-Pb ages between ~178 and 152 Ma (Pankhurst *et al*., 2000; Calderón *et al*., 2007). During the last stages of this volcanic episode, close to the eastern margin of the South Patagonian Batholith, the onset of mafic magmatism took place in an ocean floor setting, which is associated with the development of the Rocas Verdes basin. On Navarino Island these mafic volcanic rocks are included within the Tortuga Ophiolitic Complex, which has yielded U-Pb zircon ages between ~155 and 145 Ma (Calderón *et al*., 2007; Calderón *et al*., 2013). While the Rocas Verdes basin has been conventionally interpreted as a marginal basin (*e.g.* Stern and de Wit, 2003; Calderón *et al*., 2007), it has been interpreted, more recently, as

part of a triple junction associated with the opening of the southern Atlantic Ocean and the Weddell Sea (Bastias *et al*., 2021a). Nevertheless, most of the remnants of the oceanic floor of the Rocas Verdes basin are contained in the Rocas Verdes ophiolites (Stern and de Wit, 2003; Calderón *et al*. 2013), which are exposed, among other places, in the southernmost part of Navarino Island. While this unit consists of a pseudostratified complex of tholeiitic rocks including gabbros, dolerites, basalts and cherts (Suárez *et al*., 1977, 1985; Stern, 1980), on Navarino Island they consist of lavas and pillow-breccias (Suárez *et al*., 1985) with a thickness of ~1-1.5 km (de Wit and Stern, 1978).

Arc volcanic rocks formed coevally with the Rocas Verdes basalts during the Early Cretaceous (120-108 Ma). Termed the Hardy Formation (Suárez and Pettigrew, 1976), this unit includes volcaniclastic rocks, rhyolites and basalts (Suárez and Pettigrew, 1976; Suárez *et al*. 1985; Miller *et al*., 1994) and crops out on the Hardy Peninsula, Hoste Island and other nearby islands (Fig. 1). This unit represents the volcanic exposures of the Mesozoic arc.

The Rocas Verdes basin also hosts extensive turbiditic successions that have been grouped into the Yahgán Formation (Kranck, 1932; Katz and Watters, 1966; Suárez *et al*. 1985; Olivero and Martinioni, 2001), which is widely exposed in Navarino Island, Hoste Island, Isla Grande de Tierra del Fuego and other nearby islands of southern Patagonia (Fig. 1). Similarities between the depositional ages and lithofacies allow correlation of the Yahgán Formation with the Zapata, Erezcano and La Paciencia formations which are exposed elsewhere in the Tierra del Fuego region (Suárez and Pettigrew, 1976; Olivero and Malumian 2007; Poblete *et al*., 2014). Recently, Salazar *et al*. (2021) showed that the Yahgán Formation (Fig. 2) is composed of two members, based on lithological, structural, and geochronological data (zircon U-Pb LA-ICP-MS). This geochronological control is comprised of two ages - 131.4±1.3 Ma from an interbedded tuff and a maximum depositional age of 105.1±1.0 Ma obtained from detrital zircons in a sandstone. The latter constraint is similar to those presented by Barbeau *et al*. (2009) from detrital zircon ages from the northern coast of the Beagle Channel. The Yahgán Formation exhibits prehnite-pumpellyite facies metamorphism in Navarino Island (Watters, 1965; Katz and Watters, 1966).

The Rocas Verdes basin closed during the mid-Cretaceous (~100 Ma; Nelson et al., 1980; Klepeis et al., 2010) during a compressional event which was likely related to the progressive flattening of the subduction angle (Klepeis et al., 2010; Stern *et al*. 1991). This mid-Cretaceous event was also contemporaneous with an acceleration in the opening of the Atlantic Ocean and an increase in the rate of convergence between the South American and Pacific plates (*e.g.* Mpodozis and Ramos, 2008).

Furthermore, this is in agreement with paleomagnetic data suggesting an extensive tectonomagmatic event that remagnetised Jurassic and Cretaceous sedimentary and volcanic rocks (Poblete *et al*., 2011, 2016; Gao *et al*., 2021).

This mid-Cretaceous compressional event has been considered by several authors to mark the onset of the Fuegian Orogen (Bruhn, 1979; Suárez *et al*., 1985; Dalziel, 1981; Cunningham, 1994; Klepeis *et al*., 2010; Gianni *et al*., 2018, Torres Carbonell *et al*., 2020), which was associated with deformation, metamorphism and obduction in the southernmost part of Patagonia during the early Late Cretaceous. During this stage of deformation, ophiolitic complexes were obducted to the margin of South America (Katz and Watters, 1966; Calderón *et al*., 2012), whereas Klepeis *et al*. (2010) argue that obduction was linked to the southward subduction of the oceanic floor of the Rocas Verdes Basin. The contractional event occurred prior to ~86 Ma based on zircon U-Pb ages obtained from plutons that cut the regional deformation fabrics in Cordillera Darwin (Klepeis *et al*., 2010; Maloney *et al*., 2011). To the east, in the Argentine Tierra del Fuego, compression initiated later, between ~84 and 75 Ma (zircon U-Pb and hornblende $^{40}Ar/^{39}Ar$ plateau age; Gonzalez-Guillot *et al*., 2018, Torres Carbonell *et al*., 2020). This orogenic event resulted in high-pressure and Barrovian-type metamorphism of the seafloor remnants and continental basement rocks, which are exposed in Cordillera Darwin (Maloney *et al*., 2011; Calderón *et al*., 2021).

The first pulse of the Fuegian Batholith corresponds to peraluminous two-micas leucogranites and metagranites (~159-151 Ma; K-Ar and U-Pb ages; Nelson *et al*. 1980, Hervé *et al*. 1984; Klepeis *et al*., 2010; Montes, 2013). I-type, metaluminous plutons are widespread throughout the batholith. A gabbroic assemblage, which includes hornblende gabbros, diorites and hornblendites, formed between ~141 and 103 Ma (K-Ar ages, Hervé *et al*. 1984). However, Poblete *et al*. (2016) recently reported $^{40}Ar/^{39}Ar$ hornblende and biotite ages in gabbros exposed in the southern Beagle Channel, which yielded ages close to the Cretaceous–Paleocene boundary and which agree with the age presented by Torres García *et al*. (2020) on a clinopyroxene-hornblende gabbro from Hardy Peninsula, to the west of Navarino Island. The batholith is dominated by the Beagle Suite or Canal Beagle Plutonic Group (Hervé *et al*. 1984; Suárez *et al*. 1985), and is bounded by tonalites and granodiorites with strong syn- to post-deformational fabrics associated with the regional structural trends (Suárez, 1977; Suárez *et al*., 1987; Peroni, 2012; Rapalini *et al*., 2015; Poblete *et al*., 2016).

Paleocene plutons are grouped into the Seno Año Nuevo Suite (~60-34 Ma; biotite and amphibole K-Ar ages; Hervé *et al*. 1984; Suárez *et al*. 1985). This unit includes non-foliated, post-tectonic granodiorites, tonalities and quartz monzodiorites, emplaced in the southern Fuegian archipelago.

In Argentine Tierra del Fuego, small isolated plutons (such as the Ushuaia, Jeu-Jepén and Mount Krank plutons) crop out in a rear-arc setting, and are defined as the Fuegian Potassic Magmatism (FPM; González Guillot *et al*., 2009; González Guillot, 2016) (Figs. 1 and 2). The plutons are composite, ranging from hornblende clinopyroxenites, hornblendites, gabbros, monzodiorites, monzonites and syenites, with a mildly alkaline, shoshonitic composition (González Guillot *et al*., 2009). They were emplaced from ~75-68 Ma (LA-ICP-MS U-Pb zircon; Barbeau *et al*., 2009, Cerredo *et al*., 2011; González Guillot *et al*., 2018; Torres Carbonell *et al*., 2020). Another suite of plutons located in Tierra del Fuego are the high-K calc-alkaline Ushuaia Peninsula Andesites (UPA; Gonzalez Guillot *et al*. 2011, 2018), formed at ~84 Ma. They are a series of plugs and dykes of hornblendites, quartz meladiorites, granodiorites, andesites, dacites and lamprophyres.

3. Methodology

Samples from the three intrusive units (Dientes de Navarino Microdioritc Sills, Castores Plutonic Complex and Samantha Monzonites) were collected during field campaigns conducted between 2021-2018. Thin sections, whole-rock geochemistry, $^{40}Ar/^{39}Ar$ (amphibole or biotite) and zircon LA-ICP-MS U-Pb geochronology was performed at the Laboratory of SERNAGEOMIN (Servicio Nacional de Geología y Minería, Chile). Additional LA-ICP-MS zircon U-Pb geochronology of two samples was undertaken at the Department of Geology, Trinity College, Dublin, Ireland. The detailed dataset is presented in the Supplementary Material.

3.1. Petrography

Thin sections from 30 samples were studied for petrographic analysis. Characterisation was performed under a polarised light microscope to analyse their texture and mineralogy at the laboratories of SERNAGEOMIN in Santiago, Chile. The photomicrographs were obtained by a Mshot CO-90 photographic camera model MD90.

3.2. Whole-rock geochemistry

Samples were selected for whole-rock chemistry (major, trace and rare earth elements). Chemical analyses were undertaken using Agilent 7500a and 8800-QQQ inductively coupled plasma source mass spectrometry (ICP-MS) at SERNAGEOMIN. For the determination of the concentration of major oxides, glass beads were made by melting a mixture of the sample with a flux, in a 1:10 ratio. A diorite gneiss (SY-4, from the Rosenthal-Reid Lake Belt in Renfrew County, Ontario, Canada) was employed as the reference material. Trace element concentrations (Cu, V, Cr, Co, Ni, Zn, Rb, Sr, Y, Zr, Nb, Ba, Pb) were

obtained from a pressed pellet, while for the rare earth elements (REE) the solid sample underwent acid dissolution.

3.3. $^{40}Ar/^{39}Ar$ geochronology

Four samples, two hornblende-microdiorites from the Dientes de Navarino Microdioritic Sills (samples INV-05d and INS-23d), a pyroxene-biotite bearing quartz-monzonite and a hornblende bearing quartz-monzodiorite from the Samantha Monzonites (samples INV-10d and INS-10d), were selected for $^{40}Ar/^{39}Ar$ geochronology. Thin sections were first evaluated for alteration of amphibole and/or biotite. Mineral separates were obtained by milling followed by magnetic separation using a Frantz isodynamic separator, followed by mineral picking under a binocular microscope. The $^{40}Ar/^{39}Ar$ dating followed the procedure of Schaen *et al*. (2020) at the Laboratory Department of SERNAGEOMIN, which has been recently intercalibrated (Klug *et al*., 2022). The minerals were placed on a high purity aluminium disc together with the monitor mineral Fish Canyon tuff sanidine (28.201±0.046 Ma, Kuiper *et al*., 2008). Samples were degassed by step-heating with a 60 W CO_2 laser, and the extracted gas was cleaned using an ARS cryotrap (at -130 °C) and three SAES NP10 getters. Argon isotopes were analysed using a Thermo Scientific Argus VI mass spectrometer with a collector array of four faraday detectors (isotope/Ω amplifier/Name, $^{40}Ar/10^{12}$/H1, $^{39}Ar/10^{12}$/Ax, $^{38}Ar/10^{12}$/L1 and $^{37}Ar/10^{13}$/L2) and one compact discrete dynode electron multiplier detector at the low mass position. Data reduction was performed using the Mass Spec software. The apparent age obtained for each heating step considers corrections for Ar isotopes associated with atmospheric argon and argon from K, Ca and Cl irradiation (^{40}Ar, ^{39}Ar, ^{38}Ar, ^{37}Ar and ^{36}Ar). The plateau was defined by the Dalrymple and Lanphere (1974) criterion, which considers at least three consecutive steps containing at least 50% of the total ^{39}Ar released. Uncertainties overlap at the 2σ level. The age constants used are those of Steiger and Jager (1977).

3.4. Zircon U-Pb LA-ICP-MS geochronology

Samples were crushed and pulverised in a Retsch pulverizer, to a size less than 500 µm. The zircons were picked under a magnifying glass and were mounted on a 2.5 cm diameter epoxy resin disc.

The U-Pb isotopic composition of zircons from sample INS-10d (Samantha Monzonites) was obtained by LA-ICP-MS at the Isotopic Geology Laboratory of SERNAGEOMIN. Zircons were ablated using a Photon Machines Analyte G2 ArF 193 nm excimer ablation system coupled to a Thermo Element XR ICP-MS. Ablation employed the following parameters: 20 µm beam size, 10 Hz repetition rate, 30 s signal and a beam energy density of 3.8 – 4.2 J/cm^2. U, Pb and Th concentrations were calculated relative to the reference zircon GJ-1 (Jackson *et al*., 2004). Following baseline correction, the Pb/U ratios were corrected for downhole fractionation and normalised to reference zircon GJ-1.

Zircons from samples INS-45d (foliated diorite) and INS-57d (tonalite) from the Castores Plutonic Complex were dated by LA-ICP-MS using a Photon Machines Iridia 193 nm ArF Excimer laser ablation system coupled to an Agilent 7900 ICP-MS at the Department of Geology, Trinity College Dublin. The ICP-MS instrument was tuned using NIST 612 standard glass to yield Th/U ratios of unity and low oxide production rates (ThO^+/Th^+ typically less than 0.15%). 0.46 l/min He carrier gas was fed into the cell body and 0.04 l/min He was fed into the cup, and the aerosol was subsequently mixed with 0.7 l/ min Ar make-up gas and a small volume of N_2 (ca. 9 ml/min). The following twelve isotopes were measured (with their respective dwell times in milliseconds listed in parentheses): ^{49}Ti(5), ^{91}Zr(7), ^{175}Lu(7.5), ^{178}Hf(7.5), ^{202}Hg(10), ^{204}Pb(18), ^{206}Pb(45), ^{207}Pb(90), ^{208}Pb(18), ^{232}Th(18), ^{235}U(45) and ^{238}U(45). For all analyses the laser fluence was 2.25 J/cm^2, with a repetition rate of 11 Hz, a 25 µm spot size and an analysis time of 27 s, followed by a 9 s background measurement. Blocks of eight standards and two NIST612 standard glass analyses were followed by 20 unknown samples. The 91500 zircon (^{206}Pb/^{238}U TIMS age of 1065.4 ± 0.6 Ma; Wiedenbeck *et al*., 1995) were used as the primary standard. The secondary standards used to monitor consistency in the measured U–Pb dates were Plešovice zircon (^{206}Pb/^{238}U ID-TIMS age of 337.13 ± 0.37 Ma; Sláma *et al*., 2008), WRS 1348 zircon (^{206}Pb/^{238}U TIMS age of 526.26 ± 0.70 Ma; Pointon *et al*., 2012) and GZ7 zircon (^{206}Pb/^{238}U SIMS age of 530.26 ± 0.05 Ma; Nasdala *et al*., 2018). Dates were calculated using the Iolite4 software.

4. Field relationships and petrography

We recognise three Cretaceous–earliest Paleocene intrusive rock units on Navarino Island (Fig. 2): (i) the Dientes de Navarino Microdioritic Sills (DNMS); (ii) the Castores Plutonic Complex, and (iii) the Samantha Monzonites. These three intrusive units are recognized using a combination of field relationships and petrological and geochronological results.

4.1. Dientes de Navarino Microdioritic Sills

This unit is a group of sills of variable thickness (up to 300 m thick), which form an important part of the Dientes de Navarino massif (Fig. 3a) south of Puerto Williams. They were first described by Kranck (1932), and later by Katz and Watters (1966), who termed them as 'quartz dolerite sills'. They have a E-W to ESE-WNW orientation, are up to ~20 km long and are emplaced into meta-sedimentary rocks of the Cretaceous Yahgán Formation (Fig 3b and 3c). They are deformed by north-verging folds and reverse faults.

Based on field observations and petrography, two main units were recognised. The first is a group of clinopyroxene-plagioclase bearing sills, which have a thickness that ranges from a few to hundreds of meters (Figs 3c and 3e). The second group are represented by hornblende and hornblende-pyroxene bearing sills, which have a maximum thickness of three meters (Figs 3b and 3d). While hornblende-

bearing sills may also contain clinopyroxene phenocrysts, clinopyroxene-plagioclase bearing sills rarely contain hornblende either as phenocrystals or microcrystals in their groundmass. While these two units can be defined in the field, it is not possible to clearly differentiate them by geochronology, because the clinopyroxene-plagioclase bearing sills have not been dated. Therefore, herein we present the results of Dientes de Navarino Microdioritic Sills as a single unit.

Their main characteristics are that they are primarily fine- to medium-grained, grey microdiorites, diorites and diabases, with pyroxene and/or amphibole (hornblende), generally exhibiting isotropic textures. They typically have porphyritic to seriate textures, with amphibole, clinopyroxene and plagioclase phenocrysts a few millimetres in length. The groundmass is frequently composed of clinopyroxene, orthopyroxene and plagioclase (Fig. 3d-e) exhibiting fine ophitic to sub-ophitic intergrowth textures. The plagioclase phenocrysts are ~5-3 mm long and slightly altered to clay minerals and chlorite. In general, quartz is rare (<4%) and is present in interstices. The clinopyroxene is moderately uralitized, while the orthopyroxene is usually strongly affected by alteration to chlorite, calcite and titanite.

4.2. Castores Plutonic Complex

The Castores Plutonic Complex is a group of genetically related plutons (Fig. 2). Suárez *et al*. (1985) recognised these plutons exposed on the coast of northwest Navarino Island, and termed these rocks the Castores and Santa Rosa plutons and defined them as part of the Beagle Suite. In the present study, we have included the two plutonic bodies in the Castores Plutonic Complex. They are separated each other by a narrow septum (less than 1 km thick) of meta-sedimentary rocks of the Yahgán Formation and define circular bodies ~12-10 km in diameter (Suárez *et al*., 1987). The lithologies are mostly dioritic and tonalitic rocks, with a penetrative foliation and a planar orientation of tabular minerals and elongated mafic microgranular enclaves. Suárez *et al*. (1987) described a concentric foliation as a prominent feature of these rocks (Fig. 2).

The Castores Plutonic Complex intrudes the turbidites of the Yahgán Formation. The contacts are clear, with development of contact metamorphism with silicification halos and brecciation. Occasionally, the contacts of the Castores Plutonic Complex are faulted. While this unit is predominantly mesocratic foliated diorites and leucocratic tonalites (Fig. 4a), most of them hornblende-bearing, the compositions vary from hornblendites to tonalites. The hornblende diorites are medium- to coarse-grained and show a marked magmatic foliation (Fig. 5) defined by the preferential alignment of plagioclase (60-55%), amphibole (30-25%) and biotite (<5%) crystals (Fig. 5d). Further, they can vary from mesocratic to melanocratic, depending on the amount of hornblende. To the northwest of Estancia Santa Rosa (Fig. 2), the plutonic rocks show mesoscopic banding of

magmatic origin, where melanocratic facies (diorites) can be distinguished together with leucocratic facies (tonalites) (Fig. 4b), which are also locally folded. This unit also hosts leucocratic hornblende-biotite tonalites (Fig. 4a and Fig. 5e,f), which are medium grained and exhibit a moderately developed magmatic fabric (less well developed than that the hornblende diorites) with phaneritic texture and they are relatively equigranular. Tonalites have plagioclase (45-40%), quartz (25-20-%), hornblende (30-25%) and biotite (7-5%), without clear signs of alteration. The plagioclase phenocrysts (in the inequigranular varieties) sometimes have hornblende and biotite inclusions (Fig. 5f). In general, the tonalites include abundant oriented mafic microgranular enclaves (Fig. 4a) which are cut by centimetric mafic diabase dykes. These enclaves have similar lithologies to their hornblende-biotite tonalites hosts; they are rich in amphibole and biotite, suggesting the same mixing sources. Locally, the hornblende-biotite tonalites are strongly deformed to meta-tonalites with development of a proto-matrix composed by fine grains of quartz and plagioclase (Fig. 5c,d) and their mafic microgranular enclaves exhibit ductile deformation. Furthermore, Suárez *et al*. (1982) recognised foliated, folded and boudinaged tonalitic dykes, emplaced into the contact zone with the Yaghán Formation.

Gabbros (hornblende gabbros) and hornblendites are also present and they either occur as inclusions within foliated diorites and tonalites or are cut by veinlets of tonalitic composition (Fig. 4c). They are melanocratic, green to black, coarse to very coarse-grained bodies, with phaneritic and pegmatitic textures with a lack of foliation. The mineral assemblage includes inequigranular euhedral hornblende (80-60%) that is locally chloritized, late interstitial sericitized plagioclase (20-10%) and to a lesser extent clinopyroxene (5%), and trace calcite and apatite. These gabbros and hornblendites exhibit frequent and abrupt textural changes, including pegmatitic domains enriched in amphibole, and contacts with leucocratic facies (Fig. 4c) where large amphibole crystals grow perpendicular to the contacts.

4.3. Samantha Monzonites

This unit is comprised of isolated plutons and dykes emplaced within the Yahgán Formation and the Dientes de Navarino Microdioritic Sills (Fig. 2), which are similar to those described by Kranck (1932) and Katz and Watters (1966) in the south of Navarino Island. The Samantha Monzonites exhibit late-magmatic orange to red alteration zones at their contacts with the host rocks (Fig. 6a, 6b). Field observations suggest that these plutons were emplaced within pre-existing structures, favouring areas of crustal weakness (Fig. 6a). In general, the plutons are smaller than ~7 km^2, with irregular shapes, often semi-circular or elongated north-south with metric-scale dykes (Fig. 6c). These rocks differ from

the typical diorite-granodiorite-tonalite composition of the Fuegian Batholith (see Montes, 2013) and thus are particularly important for understanding the evolution of the Fuegian Andes.

They are relatively fresh leucocratic intrusive rocks with isotropic fabrics, and lack signs of metamorphism and sub-solidus fabrics. Two main facies are recognised; clinopyroxene-biotite quartz-monzonites and hornblende quartz-monzodiorites to quartz-diorites, which generally intrude the quartz-monzonites. The quartz-monzonites have a medium-grained equigranular texture, locally poikilitic (Fig. 7a,b) to slightly oriented, with magmatic flow textures. They are composed of plagioclase, pyroxene, biotite, alkali feldspar and quartz (Fig. 7). Pyroxene (12-10%) is the most abundant ferromagnesian mineral and is simple twinned and moderately uralitized and/or replaced by biotite (Fig. 7c,d). The biotite crystals (10%) host apatite and magnetite microcrystals. Plagioclase crystals are moderately sericitized, and alkali feldspar is poikilitic, encompassing pyroxene and plagioclase. The hornblende-rich quartz-monzodiorites are isotropic and equigranular coarse to medium-grained rocks with minor poikilitic textures. The plagioclase is generally fresh or slightly altered to clay minerals and calcite. Amphibole (15-10%) is euhedral (Fig. 7e,f) and generally fresh with minor chloritization and with plagioclase inclusions and typically exhibits simple twinning. The orthoclase (22-10%) is represented by irregular oikilitic crystals up to 5 mm, is anhedral and includes plagioclase and amphibole crystals. Quartz (8-6%) is scarce and is anhedral with irregular shapes. Pyroxene (2%) occurs as relicts surrounded by secondary amphibole (uralitization). Quartz-diorites have petrographic and mineralogical features similar to the hornblende-rich quartz-monzodiorites.

5. Geochemistry

Major oxides, trace element and REE whole rock data have been obtained from twenty samples, including ten from the Dientes de Navarino Microdioritic Sills, five from the Castores Plutonic Complex and five from the Samantha Monzonites. Further details on the geochemical results are listed in the Supplementary Material. The major oxide concentrations have been recalculated to 100% on an anhydrous basis, and the Fe_2O_3 and FeO abundances have been estimated from the analytical data and expressed as Fe_2O_3(T). The cationic scheme of de la Roche *et al*. (1980; Fig. 8a) suggests that Dientes de Navarino Microdioritic Sills are mostly quartz-monzonites, monzodiorites and diorites with some gabbros and granodiorites. The Castores Plutonic Complex are close to gabbroic composition and the Samantha Monzonites exhibit more felsic compositions such as monzodiorite and tonalite. However, for lithological classification purposes, we employ the modal petrographic studies described in the previous section. All intrusive rocks from Navarino Island yield magnesian compositions on the diagram of Frost *et al*. (2001; Fig. 8b), with a strong affinity with Cordilleran I-type granitoids. The Castores Plutonic Complex and the Samantha Monzonites

yield compositions in the medium-K and high-K fields of Rickwood (1989), respectively; while the Dientes de Navarino Microdioritic Sills (intermediate facies) straddle the medium-K – high-K boundary (Fig. 8c). The rocks from the Dientes de Navarino Microdioritic Sills, Castores Plutonic Complex and Samantha Monzonites span the calc-alkaline and alkali-calcic differentiation trends on the modified alkaline-lime index of Frost *et al*. (2001; Fig. 8d). A plot of K_2O *vs* Na_2O shows that all the units yield compositions in the I-type field of Chappell and White (1974; Fig. 8e). The rocks from Navarino Island yield metaluminous compositions on the Aluminium Saturation Index diagram (ASI, Maniar and Piccoli, 1989; Fig. 8f).

A plot of Sr/Y vs. Y (Fig. 8g) shows that while the Dientes de Navarino Microdioritic Sills and Samantha Monzonites straddle adakite and volcanic arc rock compositions, the Castores Plutonic Complex rocks have an exclusive adakite-like affinity. The tectonic discrimination plot of Yb+Nb *vs* Rb from Pearce *et al*. (1984; Fig. 8h) suggests that all the units considered herein have a volcanic arc granite composition. Finally, the comparison of La/Yb and Nb/Y shows that whilst Samantha Monzonites and Dientes de Navarino Microdioritic Sills yield compositions close to normal arc rocks (Fig. 8i), the Castores Plutonic Complex do not present a clear affinity. This, in combination with the adakite-like affinity of the Castores Plutonic Complex (Fig. 8g), suggest that perhaps this unit may have formed in a slightly different environment than the Dientes de Navarino Microdioritic Sills and the Samantha Monzonites. Nevertheless, when geochemical indices such as La_n/Yb_n, Sr/Y and Eu/Eu* are compared for the intrusive units of Navarino Island, it is possible to observe that they do not significantly change with time (Fig. 9), which suggest the tectonic setting did not significantly change from the Cretaceous to the early Cenozoic.

N-MORB normalised trace element abundances (values from Sun and McDonough, 1989; Fig. 10a) of the intrusive rocks from the Navarino Island show that the Dientes de Navarino Microdioritic Sills, Castores Plutonic Complex and Samantha Monzonites are relatively similar. In general, they show an enrichment in light ion lithophile elements (LILE), negative Nb and Ti anomalies which suggests that a subduction-derived component was incorporated into their source. However, it is relevant to mention that some samples do not completely follow this arc-like pattern, with some positive Sr and Ba anomalies seen. Trace element concentrations of the intrusive rocks of the Navarino Island normalised to average upper continental crust (values from Taylor and McLennan, 1995; Fig. 10c) scatter with values close to unity, as expected, suggesting a good affinity.

6. Geochronology

The new geochronological data together with those radiometric ages published by Halpern and Rex (1972) and Suárez *et al*. (1985, 1987) are presented in Table 1 and represent all the geochronological data available from Navarino Island. The full dataset containing the isotopic measurements presented in this work are provided in the Supplementary Material.

Table 1: Compilation of geochronological results from the intrusive rocks of Navarino Island.

6.1 Amphibole and biotite $^{40}Ar/^{39}Ar$ geochronology

We obtained a hornblende $^{40}Ar/^{39}Ar$ plateau age of 100.8 ± 0.8 Ma with 90% ^{39}Ar in the plateau age (Fig. 11a) from a dark-coloured dioritic sill (sample INV-05d) with acicular amphibole crystals emplaced into to the Yahgán Formation. A hornblende $^{40}Ar/^{39}Ar$ age spectrum was obtained from a folded dioritic sill (sample INS-23d) of the Dientes de Navarino Microdioritic Sills. It yielded a plateau age of 97.2±1.1 Ma with 93% of the ^{39}Ar in the plateau age (Fig. 11b). This analysis yields an older age in the first step. The INS-23d sill is interbedded between sandstones and shales of the Yahgán Formation, on the limb of an anticline. Thus, we interpret that the emplacement of the Dientes de Navarino Microdioritic Sills occurred close to the Early-Late Cretaceous boundary, at ~101-97 Ma.

A biotite $^{40}Ar/^{39}Ar$ age spectrum was obtained from a biotite-pyroxene bearing quartz-monzonite (sample INV-10d) from the Samantha Monzonites, yielding a plateau age of 66.3±0.2 Ma with 94% of the ^{39}Ar released in the age plateau (Fig. 11c). This quartz-monzonite is part of a leucocratic pluton that intrudes the Yahgán Formation, generating argillic hydrothermal alteration halos. This result nearly overlaps in age with the hornblende $^{40}Ar/^{39}Ar$ plateau age of 65.6 ± 0.4 Ma (100% of the ^{39}Ar released in the age plateau) obtained from a medium-grained hornblende bearing quartz-monzodiorite.

6.2 Zircon U-Pb geochronology

Twelve and fifty zircon grains were obtained from samples INS-57d (tonalite) and INS-45d (foliated diorite), respectively. Both constrain the crystallisation age of the Castores Plutonic Complex, which has been previously constrained by K-Ar dating to ~93-82 Ma (Suárez *et al*., 1985). The zircons are euhedral, prismatic and with well-defined crystal faces. The number of grains used to obtain the weighted $^{206}Pb/^{238}U$ mean age was four for sample INS-57d and twenty-eight for sample INS-45d (Supplementary Material). Sample INS-57d yielded a weighted mean $^{206}Pb/^{238}U$ age of 89.6±4.3 Ma (MSWD=2.1; Fig. 12a,b), and sample INS-45d yielded a weighted mean $^{206}Pb/^{238}U$ age of 87.4±0.7 Ma

(MSWD=1.2; Fig. 12 c,d). Therefore, we interpret that the crystallisation age of the Castores Plutonic Complex is ~90-87 Ma.

Twenty-five zircon grains from sample INS-10d of Samantha Monzonites were obtained from a medium-grained hornblende quartz-monzodiorite. The zircons are euhedral, prismatic and with well-defined crystal faces. The number of grains used to obtain the weighted $^{206}Pb/^{238}U$ mean age was twenty-four (see Supplementary Material; Fig. 12e,f), yielding an age of 65.6±0.5 Ma (MSWD=2.1; Fig. 12e,f). We interpret this age to be representative of the crystallisation age of the Samantha Monzonites. Furthermore, this age overlaps with the two plateau $^{40}Ar/^{39}Ar$ ages obtained from the same unit, which span ~66-65 Ma (Section 6.1).

7. Discussion

7.1 Correlations with neighbouring units

In this section we compare the field observations, lithologies, geochemistry and geochronology data of the units herein presented from Navarino Island with those intrusive units that crop out in the region to better understand the evolution of the Fuegian Andes. Furthermore, we consider the Ushuaia Pluton, Ushuaia Peninsula Andesites (González Guillot *et al*., 2011, 2018), and the Puente Quemado Gabbro (Villar *et al*., 2007; González Guillot *et al*. 2016). These units are located to the north of Beagle Channel, in the Argentine Tierra del Fuego Island (Figs. 1 and 2). This database is complemented with the results from Montes (2013) from the of Fuegian Batholith and the Tortuga Complex ophiolite (Suárez, 1977; Stern, 1980).

7.1.1. Dientes de Navarino Microdioritic Sills, Tortuga Ophiolite and Puente Quemado Gabbro

Katz and Watters (1966) assumed a mantle origin for the Dientes de Navarino Microdioritic Sills and correlated them with the ophiolites of the Tortuga Complex, which are exposed in southwestern Navarino Island (Fig. 1; Suárez, 1977). Suárez *et al*. (1985) agreed with this correlation on the basis of petrographic and geochemical data and suggested that these sills may represent late magmatic pulses associated with the Tortuga Ophiolite. However, the amphibole $^{40}Ar/^{39}Ar$ plateau ages presented in this work for the Dientes de Navarino Microdioritic Sills yield ages between ~101-97 Ma, which are at least ~34 Myr younger than the ophiolitic complexes assuming the ~135 Ma U-Pb zircon maximum deposition age (Calderon *et al*., 2013) from a chert approximates the true age. This age for the Dientes de Navarino Microdioritic Sills is consistent with stratigraphic relationships, since the Tortuga Ophiolite underlies the Cretaceous Yahgán Formation and both units are cut by the Dientes de

Navarino Microdioritic Sills. Petrographically, some facies of the Dientes de Navarino Microdioritic Sills are rich in hornblende, whereas gabbros of the Tortuga Ophiolite have a primary mineralogical assemblage of clinopyroxene-plagioclase +/- olivine. This, in combination with the geochemical analysis herein presented, it suggests that the Dientes de Navarino Microdioritic Sills formed in an active margin setting.

The Puente Quemado Gabbro is comprised of thick tholeiitic mafic sills trending ~NNW (González Guillot *et al*., 2016). They include clinopyroxene-plagioclase with minor ilmenite, titanite, hornblende and apatite. While the Puente Quemado Gabbro lacks geochronological control, we speculate that it may be contemporaneous to Dientes de Navarino Microdioritic Sills, on the basis of its emplacement into the Yahgán Formation and it was similarly affected by contractional tectonics. Furthermore, these units have notable field and lithologic similarities. They also share some geochemical features, such as low La/Nb and Sr, and high Zr, Nb, Hf, Y, MREE, HREE and TiO_2/P_2O_5. However, there are geochemical differences that hamper their correlation, including the Dientes de Navarino Microdioritic Sills yielding lower Fe#, TiO_2, Ba/Th, and higher LREE, Th, Rb, La/Yb (Fig. 8i), Th/Yb, Nb/Yb. While these differences may be the result of magmatic fractionation, further studies are required to explore this correlation.

7.1.2. Castores Plutonic Complex and Ushuaia Peninsula Andesites

The Ushuaia Peninsula Andesites were emplaced at ~84 Ma (U-Pb zircon; González Guillot *et al*., 2011, 2018) and are metaluminous, calc-alkaline, and straddle the medium-K and high-K boundary on a SiO_2-K_2O diagram (Fig. 8c-f; González Guillot *et al*., 2011). They yield similar magnesian compositions to those of the Castores Plutonic Complex (Fig. 8b) along with an adakitic affinity (Fig. 8g). Some geochemical features observed in the Ushuaia Peninsula Andesites are also observed in the Castores Plutonic Complex, such as high Zr and Nb abundances, high Nb/Y and La/Yb (Fig. 8i; González Guillot *et al*., 2011). However, the Castores Plutonic Complex yield higher MREE, HREE contents, a higher Pb/Th ratio, and lower Th, Th/Hf, Th/Nb and Ba/La ratios. Although the Castores Plutonic Complex yield a slightly older age (~90-87 Ma) compared to the Ushuaia Peninsula Andesites (~84 Ma), its geographic proximity along with their geochemical affinity suggest a link between these units. Accordingly, we suggest that the Ushuaia Peninsula Andesites represent a peripheral apophyses of the later stages of the Castores Plutonic Complex magmatism.

7.1.3. Samantha Monzonites, Fuegian Potassic Magmatism and monzonites of southern Navarino Island

González Guillot (2016) suggested a correlation between the monzonites of Navarino Island with the Fuegian Potassic Magmatism on the basis of lithological similarities. However, while the Fuegian

Potassic Magmatism exhibits a monzonitic to mildly-alkaline trend (e.g. González Guillot, 2016) and plot in the ferroan field (Fig. 8b), the Samantha Monzonites mainly yield calc-alkaline and magnesian compositions. Furthermore, they also differ in age, as the Samantha Monzonites formed at ~66-65 Ma and the Fuegian Potassic Magmatism was active at ~75-68 Ma (Barbeau *et al*., 2009, Cerredo *et al*., 2011; González Guillot *et al*., 2018; Torres Carbonell *et al*., 2020). These two aspects, i.e. timing and geochemical compositions, precludes further correlation between these units. However, the Samantha Monzonites can be lithologically and petrographically correlated with the monzonites described by Kranck (1932) and Katz and Watters (1966) in the south of Navarino Island, but further work is required to prove this correlation.

Finally, the Samantha Monzonites are older than the Seno Año Nuevo Suite from the Fuegian Batholith, with these units forming at ~66-65 Ma and ~60-34 Ma (Hervé *et al*., 1984), respectively. Additionally, they also differ in their lithologies, with the Seno Año Nuevo Suite dominated by 'Andean' lithological types, such as granodiorites, tonalites and quartz-monzodiorites (with hornblende-biotite, without pyroxene). Therefore, we suggest that the Samantha Monzonites, and possibly the monzonites from southern Navarino Island as well, are an independent suite within the Fuegian Batholith.

7.2. The timing of deformation on Navarino Island

Three main stages have been recognised for the tectonic evolution of the Rocas Verdes Basin, based on their petrological, geochronological, metamorphic, structural and sedimentological constraints. They are (i) back-arc development between ~140 and 120 Ma (Calderon *et al*., 2013), (ii) tectonic inversion and basin closure between ~120 and 100 Ma (Kohn *et al*., 1995; McAtammey *et al*., 2011; Malkowsky *et al*., 2017) and (iii) Cordilleran arc collision, between ~100 and 74 Ma (Calderon *et al*., 2013, Torres Carbonell *et al*., 2020). The latter stage is associated with the obduction of the oceanic floor of the Rocas Verdes Basin (Klepeis *et al*., 2010) and the initiation of the Magallanes fold-and-thrust belt and its development from the Maastrichtian to the Miocene (Fig. 13; Torres Carbonell *et al*., 2020; Mosqueira *et al*., 2021). The Dientes de Navarino Microdioritic Sills were emplaced at ~101-97 Ma, following the ocean-floor metamorphism recorded in the Tortuga Ophiolitic Complex (~118 Ma, U-Pb titanite; Calderon *et al*., 2013), which has been interpreted as the closure stage of the Rocas Verdes basin. These sills, along with their country rock, the Yahgán Formation, were underwent contraction prior to intrusion of the isotropic plutons of the Samantha Monzonites (~66-65 Ma). Therefore, the Samantha Monzonites are post-tectonic plutons lacking ductile deformation, whose emplacement may have been facilitated by the regional structures (Fig. 6b). Hence, the contractional deformation recognised on the Navarino Island took place somewhere between ~100 and 66 Ma. This is consistent with the strongly foliated fabrics within the Castores Plutonic Complex, which suggests

emplacement under the influence of contraction during ~90-85 Ma. This deformation event is contemporaneous with the development of a ~400 km long lithospheric-scale structure in the northern segment of the Rocas Verdes basin (Muller *et al.*, 2021), and accommodates east- and northeast-verging shearing between ~100 and 80 Ma (Muller *et al.*, 2021). Additional compressional events between ~85 and 66 Ma in Navarino Island may have occurred (Fig.13), a period for which we lack deformation markers, although a compressional phase has been recently constrained further east, in Argentinian Tierra del Fuego (~84-75 Ma, Torres Carbonell et al., 2020). Summarising, the three Cretaceous-earliest Palaeocene plutonic pulses recorded in Navarino Island are pre-, syn- and post-tectonic (Fig. 14) with respect to a major compressional event caused by the Cordilleran arc-continent collision and obduction of the Rocas Verdes back arc oceanic floor.

7.3. Cretaceous tectono-magmatic evolution of the Southern Fuegian Andes

A combination of the field characteristics, petrography, geochemistry and geochronological data of the Cretaceous-earliest Paleocene igneous rocks exposed in Navarino Island suggests they all formed in a continental arc setting during the early stages of the Fuegian Orogen (Figs 6,7,8). This interpretation agrees with previous studies that suggested that Cretaceous intrusive rocks of the Fuegian Batholith originated in an active margin environment (Hervé *et al*., 1984; Montes *et al*., 2013). Our data show that a supra-subduction zone origin is supported by the hornblende and hornblende-biotite paragenesis, enriched LILE and LREE, with negative Nb, Sr and Ti anomalies (Figs. 8 and 10) in most of the studied rocks, which are typical of slab-dehydration reactions and thus active margins. A lack of temporal trends in the La_n/Yb_n, Sr/Y and Eu/Eu* plots (Fig. 9) through the ~100 to 65 Ma time window suggest that the crustal thickness of the arc did not significantly change during this period (e.g. Hildreth & Moorbath, 1988; Mantle & Collins, 2008; Chiaradia, 2015; Chapman *et al*., 2015). However, we observed for Castores Plutonic Complex and Ushuaia Peninsula Andesites relatively higher Nb/Y and La/Yb ratios (Fig. 8) with respect to the rest of Fuegian Batholith (Dientes de Navarino Microdioritic Sills and Samantha Monzonites included). This suggests that, relatively, the Castores Plutonic Complex and Ushuaia Peninsula Andesites, have an significant incorporation of garnet-stable melts in the asthenospheric wedge (Martin et al., 2005; Rapp et al., 2006), which may be accounted for by differences in the crustal thickness during ~90-84 Ma. Nevertheless, we acknowledge that estimates of the thickness of continental arc crust using geochemical indices are problematic due to the multiple petrogenetic processes that occur in this setting (Ducea *et al*., 2015), and these should perhaps only be used as qualitative indicators (e.g. Kay & Mpodozis, 2001; Best *et al*., 2009; Oliveros *et al*., 2018). The trace element compositions of Cretaceous igneous rocks to the north of Beagle

Channel (the Ushuaia Pluton of the Fuegian Potassic Magmatism and the calc-alkaline Ushuaia Peninsula Andesites) yield similar compositions with respect to those present on Navarino Island (Figs. 8, 9, 11), and thus likely also formed under the influence of an active margin setting. However, we also acknowledge that there are differences in the magmatic style. The Dientes de Navarino Microdiorite Sills are hornblende- and/or clinopyroxene-bearing dioritic hypabyssal rocks (sills and dykes), the Castores Plutonic Complex is a suite of variably foliated, hornblende- / biotite-bearing gabbroic to tonalitic plutons and the Samantha Monzonites are isolated plutons of monzonitic to monzodioritic composition containing pyroxene and minor hornblende-biotite.

On a regional scale, after the back-arc stage of the Rocas Vardes basin (Fig. 14a) at 140-120 Ma, the magmatic rocks associated with the active margin migrate with time. From the mid-Cretaceous to the Cretaceous-Paleocene boundary, the magmas clearly migrate north to northeast (*e.g.* Stern, 1991; Folguera and Ramos, 2011; Gonzalez Guillot *et al*., 2011, 2018). This migration is contemporaneous with the early stages of compressional tectonic events which have been related to the closure of the Rocas Verdes marginal basin ~120-100 Ma (see Fig. 14b, and Klepeis *et al*., 2010; McAtammey *et al*., 2011; Kohn *et al*., 1995; Calderón *et al*., 2013), the obduction of the Tortuga Ophiolitic Complex, which corresponds to the initial development of the foreland basin (~100-80 Ma; Calderón *et al*., 2013; Muller *et al*., 2021) and the initial development of the Fuegian Fold and Thrust belt (Maastrichtian-Danian, Torres Carbonell *et al*., 2020; Mosqueira *et al*., 2021). This period encompasses the emplacement of the Dientes de Navarino Microdioritic Sills (Fig. 14b), which record the onset of the Cretaceous intrusive magmatism on Navarino Island (~101-97 Ma) and is contemporaneous with pluton emplacement further northwest in the Cordillera Darwin (Fig. 13). The Castores Plutonic Complex (~90-87 Ma) spatially overlaps with the Dientes de Navarino Microdioritic Sills (Figs. 2 and 14c). Subsequent magmatic events include the calc-alkaline Ushuaia Peninsula Andesites (~84 Ma, González Guillot *et al*., 2018), other calc-alkaline plutons of the Beagle Suite (~86-74 Ma; e.g., Klepeis *et al*., 2010, McAtamney *et al*., 2011) and the shoshonitic Fuegian Potassic Magmatism (~75-68 Ma, e.g. González Guillot *et al*., 2018; Torres Carbonell *et al*., 2020) seen on Argentine Tierra del Fuego (Fig. 14d), with some plutons located up to 45 km to the north of Navarino Island. This implies arc widening (or expansion) to the north throughout the Late Cretaceous (Fig. 13 and Fig. 14 c,d) related to the decrease of the dip of the Benioff zone. This is followed by significant migration towards the trench after ~68-66 Ma, which places the arc magmatism in southwest Navarino Island and further south in the Seno de Año Nuevo Suite, where it remained until the Eocene (Hervé *et al*., 1984)., suggesting south-directed migration towards the trench (Fig. 14e). Regionally, these Paleocene-Eocene plutons generally are located to the south of ophiolitic complexes (Suárez et al., 1985). Other plutons located further south, such as the monzonites of Grandi River (Kranck, 1932) and Paleocene

plutons of Hardy Peninsula (Torres García *et al*., 2020) may represent other magmatic pulses associated with this event. While the mechanism responsible for this change is uncertain, we speculate that a change in the subduction angle may be responsible. This change could be related to a change in plate configuration between 80 to 60 Ma due to the southward migration of the Antarctic Peninsula relative to southernmost Patagonia (Merdith et al., 2021). However, this potential change in the subduction angle needs be explored further.

8. Conclusions

Navarino Island hosts three main magmatic units that were emplaced during the Cretaceous to earliest Palaeocene times between 101 and 65 Ma. They are the (i) Dientes de Navarino Microdioritic Sills emplaced at ~101-97 Ma (hornblende $^{40}Ar/^{39}Ar$ ages), (ii) the Castores Plutonic Complex that formed during ~90-87 Ma (zircon U-Pb ages), and (iii) the Samantha Monzonites which were emplaced at ~66-65 Ma (hornblende and biotite $^{40}Ar/^{39}Ar$ and zircon U-Pb ages). Geochemical compositions of these rocks suggest that they formed above an active subduction zone, forming part of the Fuegian Batholith, to the south of the Fuegian Potassic Magmatism of Argentinian Tierra del Fuego. The arc suites of Navarino Island show differences in their modes and timings of emplacement, lithologies and petrography. The Dientes de Navarino Microdioritic Sills are pre-tectonic hornblende- and/or clinopyroxene-bearing microdioritic hypabyssal rocks, showing a similar deformation style to that observed in the Lower Cretaceous Yahgán Formation country rocks. The Castores Plutonic Complex are a group of pre- to syn-tectonic hornblende-biotite gabbroic to tonalitic plutons, with a predominance of hornblende-bearing quartz-diorites, occasionally with development of intense magmatic and deformative fabrics. Finally, the Samantha Monzonites are isolated, non-deformed monzonitic to monzodioritic post-tectonic plutons, emplaced along pre-existing structures, containing pyroxene and minor hornblende-biotite, associated with hydrothermal alteration zones. Although the three units recognised in Navarino Island geographically overlap, the Late Cretaceous magmatism shows an overall widening to the northeast in the Fuegian Andes. This is observed from ~101 to ~68 Ma and is followed by a southward migration during ~68-66 Ma, which is represented by the Samantha Monzonites (~66-65 Ma) and other Paleocene plutons located to the south of Beagle Channel (Hoste Island). While this suggests that the Fuegian Andes arc magmatism experienced expansion at an early stage of development, it remains unclear which mechanism provoked the trench-ward migration at ~ 68-66 Ma.

Acknowledgements

This research was funded by the Plan Nacional de Geología of SERNAGEOMIN (Chilean Geological and Mining Survey) and grants from Universidad de O'Higgins and Universidad de Chile. We thank El Padrino camping and Cecilia from Puerto Williams. P. Duhart, J. Rodrigo, R. González and C. Loidoy are thanked for their help in the field. JB was funded by the Swiss National Science Foundation (project P500PN_202847). DC acknowledges support from Science Foundation Ireland (SFI) under Grant Number 13/RC/2092 and 13/RC/2092_P2 (SFI Research Centre in Applied Geosciences, iCRAG). M. Ghiglione is thanked for editorial handling, and the authors are grateful to two anonymous reviewers for the constructive comments.

References

Acevedo R., Linares E., Ostera H., Valín-Alberdi M. (2002) La Hornblendita Ushuaia (Tierra del Fuego): Geoquímica y Geocronología. Rev Asoc Geol Argentina 57(2):133–142

Barbeau D.; Gombosi D.: Zahid K.;, Bizimis M.;, Swanson-Hysell N.;, Valencia V.; Gehrels G. 2009. U-Pb zircon constraints on the age and provenance of the Rocas Verdes basin-fill, Tierra del Fuego. Argentina. Geochem Geophys Geosys 10:Q12001.

Bastias, J., Spikings, R., Riley, T., Ulianov, A., Grunow, A., Chiaradia, M., & Hervé, F. 2021a. A revised interpretation of the Chon Aike magmatic province: active margin origin and implications for the opening of the Weddell Sea. Lithos, 386, 106013.

Bastias, J., Spikings, R., Riley, T., Ulianov, A., Grunow, A., Chiaradia, M., & Hervé, F. 2021b. Data on the arc magmatism developed in the Antarctic Peninsula and Patagonia during the Late Triassic–Jurassic: A compilation of new and previous geochronology, geochemistry and isotopic tracing results. Data in brief, 36, 107042.

Best, M. G., Barr, D. L., Christiansen, E. H., Gromme, S., Deino, A. L., & Tingey, D. G. (2009). The Great Basin Altiplano during the middle Cenozoic ignimbrite flareup: Insights from volcanic rocks. International Geology Review, 51(7-8), 589-633.

Boekhout, F., Spikings, R., Sempere, T., Chiaradia,M., Ulianov, A., Schaltegger, U., 2012. Mesozoic arc magmatism along the southern Peruvian margin during Gondwana breakup and dispersal. Lithos 146–147, 48–64.

Bruhn, R.L., Stern, C.R., de Wit, M.J., 1978. Field and geochemical data bearing on the development of a Mesozoic volcano-tectonic rift zone and back-arc basin in southernmost South America. Earth Planet. Sci. Lett. 41, 32–46.

Caminos, R. 1980. Cordillera Fueguina. En Turner, J. (coord.) Segundo Simposio de Geología Regional Argentina, Academia Nacional de Ciencias 2: 1463-1501, Córdoba.

Cao, S.J., Torres Carbonell, P.J., Dimieri, L.V. 2018. Structural and petrographic constraints on the stratigraphy of the Lapataia Formation, with implications for the tectonic evolution of the Fuegian Andes. Jr. South Amer. Earth Sciences 84, 223-241. doi:https://doi.org/10.1016/j.jsames.2018.04.002.

Calderon, M.; Fildani, A.; Hervé, F.; Fanning, M.; Weislogel, A.; Cordani, U. 2007. Late Jurassic bimodal magmatism in the northern sea-floor remnant of the Rocas Verdes basin, southern Patagonian Andes. Journal of the geological Society 164: 1011-1022.

Calderon, M., Fosdick, J.C., Warren, C., Massonne, H.-J., Fanning, C.M., Fadel Cury, L., Schwanethal, J., Fonseca, P.E., Galaz, G., Gaytán, D., Hervé, F., 2012. The low-grade Canal de las Montañas Shear Zone and its role on the tectonic emplacement of the Sarmiento Ophiolitic Complex and Late Cretaceous Patagonian Andes orogeny, Chile. Tectonophysics 524–525, 165–185.

Calderon, M.; Prades, C.F.; Hervé, F.; Avendaño, V.; Fanning, M.C.; Massone, H-J.; Theye, T.; Simonetti, A. 2013. Petrological vestiges of the Late Jurassic-Early Cretaceous transition from rift to back-arc basin in southernmost Chile: New age and geochemical data from the Capitán Aracena, Calos II and Tortuga ophiolitic complex. Geochemical Journal 47: 201-2017.

Calderon, M., Zúñiga, C., Hervé, F., Theye, T., Galaz, G., Rojo, D., and Suárez, R.: Barrovian-type metamorphism in the western domain of the Cordillera Darwin Metamorphic Complex, Fuegian Andes, EGU General Assembly 2021, online, 19–30 Apr 2021, EGU21-5612, https://doi.org/10.5194/egusphere-egu21-5612, 2021.

Caminos, R. 1980. Cordillera Fueguina. En Turner, J. (coord.) Segundo Simposio de Geología Regional Argentina, Academia Nacional de Ciencias 2: 1463-1501, Córdoba.

Cao, S.J., Torres Carbonell, P.J., Dimieri, L.V. 2018. Structural and petrographic constraints on the stratigraphy of the Lapataia Formation, with implications for the tectonic evolution of the Fuegian Andes. Jr. South Amer. Earth Sciences 84, 223-241. doi:https://doi.org/10.1016/j.jsames.2018.04.002.

Cerredo M., Tassone A., Rapalini A., Hervé F., Fanning M. (2011). Campanian magmatism in the Fuegian Andes: new SHRIMP age of JeuJepen pluton. Argentina. XVIII Argentinian Geological Congress, Neuquén, pp 714–715

Chapman, J. B., Ducea, M. N., DeCelles, P. G., & Profeta, L. (2015). Tracking changes in crustal thickness during orogenic evolution with Sr/Y: An example from the North American Cordillera. Geology, 43(10), 919-922.

Chappell, B.W., White, A.J.R., 1974. Two contrasting granite types. Pac. Geol. 8, 173–174.

Chiaradia, M. (2015). Crustal thickness control on Sr/Y signatures of recent arc magmas: an Earth scale perspective. Scientific reports, 5(1), 1-5.

Cunningham, W.D., 1994. Uplifted ophiolitic rocks on Isla Gordon, southernmost Chile: Implications for the closure history of the Rocas Verdes marginal basin and the tectonic evolution of the Beagle Channel region. J. S. Am. Earth Sci. 7, 135–147.

Dalrymple, G. B., & Lanphere, M. A. (1974). 40Ar/39Ar age spectra of some undisturbed terrestrial samples. Geochimica et Cosmochimica Acta, 38(5), 715-738.

Dalziel, I. 1981. Back arc extension in the southern Andes, a review and critical reappraisal. Philosophical Transaction of the Royal Society of London, Series A, 300: 319-335.

deWit, M.; Stern, C. 1978. Variations in the degree of crustal extension during formation of back-arc basin. Tectonophysics, Vol. 72, p. 229-260.

de La Roche, H., Leterrier, J., Grandclaude, P.,Marchal,M., 1980. A classification of volcanic and plutonic rocks using R1R2-diagram and major-element analyses - its relationships with current nomenclature. Chem. Geol. 29, 183–210.

Ducea, M. N., Otamendi, J. E., Bergantz, G. W., Jianu, D., & Petrescu, L. (2015). The origin and petrologic evolution of the Ordovician Famatinian-Puna arc. Geological Society of America Memoirs, 212, 125-138.

Defant, M.J. and Drummond, M.S. (1990) Derivation of Some Modern Arc Magmas by Melting of Young Subducted Lithosphere. Nature, 347, 662-665. https://doi.org/10.1038/347662a0

Fleck, R., Sutter, J., Elliot, D. Interpretation of discordant 40Ar/39Ar age-spectra of mesozoic tholeiites from antarctica, Geochimica et Cosmochimica Acta, Volume 41, Issue 1, 1977, Pages 15-32, ISSN 0016-7037, https://doi.org/10.1016/0016-7037(77)90184-3.

Folguera A., Ramos V. (2011) Repeated eastward shifts of arc magmatism in the Southern Andes: a revision to the long-term pattern of Andean uplift and Magmatism. J S Am Earth Sci 32(4):531–546

Frost, B., Barnes, C., Collins,W., Arculus, R., Ellis, D., Frost, C. 2001. A Geochemical classification of granitic rocks. J. Petrol. 42, 2033–2048. https://doi.org/10.1093/petrology/ 42.11.2033.

Gao, L., Pei, J., Zhao, Y., Yang, Z., Riley, T. R., Liu, X., ... & Liu, J. M. (2021). New paleomagnetic constraints on the Cretaceous tectonic framework of the Antarctic Peninsula. Journal of Geophysical Research: Solid Earth, 126(11), e2021JB022503.

Gianni, G. M., Pesce, A., & Soler, S. R. (2018). Transient plate contraction between two simultaneous slab windows: Insights from Palaeocene tectonics of the Patagonian Andes. Journal of Geodynamics, 121, 64-75.

González Guillot, M.; Escayola, M.; Acevedo, R.; Pimentel, M.; Seraphim, G.; Proenza, J. y Schalamuk, I. 2009. The Plutón Diorítico Moat: mildly alkaline monzonitic magmatism in the Fuegian Andes of Argentina. Journal of South American Earth Sciences, 28: 345-359, doi: 10.1016/j.jsames.2009.04.006.

González Guillot, M.; Escayola, M.; Acevedo, R. 2011. Calc-alkaline rear-arc magmatism in the Fuegian Andes: Implications for the mid-cretaceous tectonomagmatic evolution of southernmost South America. Journal of South American Earth Sciences 31: 1-16.

González Guillot M.; Prezzi C.; Acevedo R.D:; Escayola M. 2012. A comparative study of two rear-arc plutons and implications for the Fuegian Andes tectonic evolution: Mount Kranck Pluton and Jeu-Jepén Monzonite, Argentina. J S Am Earth Sci 38:71–88.

González Guillot, M.; Urraza, I.; Acevedo, R.; Escayola, M. 2016. Magmatismo básico Jurásico-Cretácico de los Andes Fueguinos y su relación con la cuenca marginal Rocas Verdes. Rev. Asoc. Geol. Argentina, 73(1): 1-22.

González Guillot, M.; Ghiglione, M.; Escayola, M.; Martins Pimentel, M.; Mortensen, J.; Acevedo, R. 2018. Ushuaia pluton: Magma diversification, emplacement and relation with regional tectonics in the southernmost Andes. Journal of South American Earth Sciences 88: 497-519.

González Guillot, M., 2016. Magmatic evolution of the southernmost Andes and its relation with subduction processes. In: Ghiglione, M. (Ed.), Geodynamic Evolution of the Southernmost Andes: Connections with the Scotia Arc. Springer International Publishing, pp. 37–74 ISBN: 978-3-319-39725-2.

Halpern M.;, Rex D.C. 1972. Time of folding of the Yahgán Formation and age of the Tekenika beds, Southern Chile, South America. Geol Soc Am Bull 83:1881–1886

Hervé, M.; Suárez, M.; Puig, A. 1984. The Patagonian Batholith S of Tierra del Fuego, Chile: timing and tectonic implications. Journal of the Geological Society of London 141: 909-917.

Hervé, F.; Fanning, C.M.; Pankhurst, R.J.; Mpodozis, C.; Klepeis, K.; Calderón, M.; Thomson, S.N. 2010. Detrital zircon SHRIMP U–Pb age study of the Cordillera Darwin Metamorphic Complex of Tierra del Fuego: sedimentary sources and implications for the evolution of the Pacific margin of Gondwana. Journal of the Geological Society 167 (3): 555-568.

Hervé, F., Pankhurst, R.J., Fanning, C.M., Calderón, M., Yaxley, G.M., 2007. The South Patagonian batholith: 150 my of granite magmatism on a plate margin. Lithos 97, 373–394

Hildreth, W.S. and Moorbath, S. (1988) Crustal Contribution to Arc Magmatism in the Andes of Central Chile. Contributions to Mineralogy and Petrology, 98, 455-489. http://dx.doi.org/10.1007/BF00372365

Jackson, S. E., Pearson, N. J., Griffin, W. L., & Belousova, E. A. (2004). The application of laser ablation-inductively coupled plasma-mass spectrometry to in situ U–Pb zircon geochronology. Chemical geology, 211(1-2), 47-69.

Jackson, S.E., 2008. Lamtrace data reduction software for LA-ICP-MS. In: Sylvester, P. (Ed.), Laser Ablation ICP-MS in the Earth Sciences: Current Practices and Outstanding Issues. Short Course Series, Vol. 40. Mineralogical Association of Canada, pp. 305–307.

Katz, H.R.; Watters, W.A. 1966. Geological investigation of the Yahgán Formation (Upper Mesozoic) and associated igneous rocks of the Navarino Island, Southern Chile. New Zealnd Journal of the geology and Geophysics 9 (3): 323-359.

Kay, S.M., Mpodozis, C., 2001. Central Andean ore deposits linked to evolving shallow subduction systems and thickening crust. GSA Today 11, 4-9

Klepeis K, Betka P, Clarke G, Fanning M, Hervé F, Rojas L, Mpodozis C, Thomson S (2010) Continental underthrusting and obduction during the Cretaceous closure of the Rocas Verdes rift basin, Cordillera Darwin, Patagonian Andes. Tectonics 29 TC3014.

Klug, J.; Ramirez, A.; Singer, B.; Jicha, B.; Mixon, E.; Martinez, P. 2022. Intercalibration of the Servicio Nacional de Geología y Minería (SERNAGEOMIN), Chile and WiscAr 40Ar/39Ar laboratories for Quaternary dating. Quaternary Geochronology, Volume 72, 2022, 101354, ISSN 1871-1014.

Kohn, M.J., Spear, F.S., Harrison, T.M., Dalziel, I.W.D., 1995. 40Ar/39Ar geochronology and P-T-t paths from the Cordillera Darwin metamorphic complex, Tierra del Fuego, Chile. J. Metamorph. Geol. 13, 251–270.

Kranck, H.E. 1932. The Coast Cordillera South of Tierra del Fuego. Acta Geographica 4 (2): 115-137.

Kuiper, K., Deino, A., Hilgen, F., Krijgsman, W., Renne, P., and Wijbrans, J.R., 2008, Synchronizing Rock Clocks of Earth History: Science, v. 320, p. 500–504. doi:10.1126/ science.1154339. Landenberg and Collins. 1996

Maloney, K., Clarke, G., Klepeis, K., Fanning, C., Wang, W., 2011. Crustal growth during back-arc closure: Cretaceous exhumations history of Cordillera Darwin, southern Patagonia. J. Metamorph. Geol. 29, 649–672.

Martin, H., Moyen, J.-F., Rapp, R., 2010. The sanukitoid series: magmatism at the Archaean-Proterozoic transition. Earth and Environmental Science Transactions of the Royal Society of Edinburgh 100, 15e33.

McAtamney J, Klepeis K, Mehrtens C, Thomson S, Betka P, Rojas L, Snyder S (2011) Along-strike variability of back-arc basin collapse and the initiation of sedimentation in the Magallanes foreland basin, Southernmost Andes (53–54.5°S). Tectonics 30 TC5001

Maniar, P.D.; Piccoli, P.M. 1989. Tectonic discrimination of granitoids. Geol. Soc. Am. Bull. 101, 635–643. https://doi.org/10.1130/0016- 606(1989)101b0635.

Miller C., Barton M, Hanson RE, Fleming TH.1994. An Early Cretaceous volcanic arc/marginal basin transition zone, Peninsula Hardy, southernmost Chile. J Volcanol Geoth Res 63(1–2): 33–58.

Martin, H, Smithies, R.H., Rapp, R., Moyen, J-F., Champion, D. 2005. An overview of adakite, tonalite–trondhjemite–granodiorite (TTG), and sanukitoid: relationships and some implications for crustal evolution. Lithos, 79 (2005), pp. 1-24.

Merdith, A., Williams, S., Collins, A., Tetley, M., Mulder, J., Blades, M., Young, A., Armistead, S., Cannon, J., Zahirovic, S., Müller, D. 2021. Extending full-plate tectonic models into deep time: Linking the Neoproterozoic and the Phanerozoic, Earth-Science Reviews, Volume 214, 2021, 103477, ISSN 0012-8252, https://doi.org/10.1016/j.earscirev.2020.103477.

Montes, M., Hervé, F., Calderón, M., Fanning, C. M., Ramírez de Arellano. C. 2013. Magmatic Evolution of the Fuegian Batholith, southernmost Chile at 53º–56ºS: Tectonic Implications. Bollettino di Geofisica Nº 54 Supl. 2, p. 333-334Montes, M. 2013. Evolución magmática del Batolito Fuegiano, XII Región de Magallanes y de la Antártica chilena, Chile. Memoria de Título, Universidad de Chile, Departamento de Geología.

Mosqueira V., Torres Carbonell, P., Turienzo, M. 2021. Structural overprinting and style of deformation at sierra Beauvoir and sierra de Apen: A geometric and kinematic model for the evolution of the internal thrust-fold belt, Fuegian Andes, Argentina, Journal of South American Earth Sciences, Volume 112, Part 1, 2021, 103575, ISSN 0895-9811, https://doi.org/10.1016/j.jsames.2021.103575.

Mpodozis, C., Ramos, V., 2008. Tectónica jurásica en Argentina y Chile: Extensión, subducción oblicua, rifting, deriva y colisiones? Rev. Asoc. Geol. Argentina 63 (4), 481e497.

Nasdala, L., Corfu, F., Schoene, B., Tapster, S. R., Wall, C. J., Schmitz, M. D., ... & Giester, G. (2018). GZ 7 and GZ 8–Two Zircon Reference Materials for SIMS U-Pb Geochronology. Geostandards and Geoanalytical Research, 42(4), 431-457.

Nelson EP, Dalziel IWD, Milnes AG (1980) Structural geology of the Cordillera Darwin-collision style orogenesis in the Southernmost Andes. Eclogae Geol Helv 73:727–751

Olivero E. and Martinioni D. 2001. A review of the geology of the Argentinian Fuegian Andes. *Journal of South American Earth Science*, **14**, 175–188, https://doi.org/10.1016/S0895-9811(01)00016-5

Oliveros, V., González, J., Espinoza, M., Vásquez, P., Rossel, P., Creixell, C., Sepúlveda, F., Bastías, F., 2018. The early stages of the magmatic arc in the Southern Central Andes. In: Folguera, *et al*. (Eds.), The Evolution of the Chilean-Argentinean Andes. Springer, Berlín , pp. 185–212. ttps://link.springer.com/chapter/10.1007/978-3- 319-67774-3_7.

Olivero, E., Malumián N. 2007. Mesozoic-Cenozoic stratigraphy of the Fuegian Andes Argentina. Geologica Acta 6(1):5–18
Olivero E., Martinioni D. 2001. A review of the geology of the Argentinian Fuegian Andes. Journal of South American Earth Science 14: 175–188

Pankhurst, R.J., Riley, T.R., Fanning, C.M., Kelley, S.P., 2000. Episodic silicic volcanism in Patagonia and the Antarctic Peninsula: chronology of magmatism associated with the break– up of Gondwana. J. Petrol. 41, 605–625.

Peacock, M.A., 1931. Classification of igneous rock series. J. Geol. 39, 54–67.

Pearce, J.A., Harris, N.B.W., Tindle, A.G., 1984. Trace element discrimination diagrams for the tectonic interpretation of granitic rocks. J. Petrol. 25, 956–983.

Peroni, J. 2012. Modelado geofísico-geológico de plutones en las Islas Grande de Tierra del Fuego (Argentina) y Navarino (Chile). Facultad de Ciencias Exactas y Naturales. Universidad de Buenos Aires.

Poblete, F., Arriagada, C., Roperch, P., Astudillo, N., Hervé, F., Kraus, S., & Le Roux, J. P. 2011. Paleomagnetism and tectonics of the South Shetland Islands and the northern Antarctic Peninsula. Earth and Planetary Science Letters, 302(3-4), 299-313.

Poblete, F.; Roperch, P.; Arriagada, C.; Ruffet, G.; Ramírez de Arellano, C.; Hervé, F.; Poujol, M. 2016. Late Cretaceous-early Eocene counterclockwise rotation of the Fuegian Andes and evolution of the Patagonia-Antarctic Peninsula system. Tectonophysics.

Poblete, F., Roperch, P., Hervé, F., Diraison, M., Espinoza, M., & Arriagada, C. 2014. The curved Magallanes fold and thrust belt: Tectonic insights from a paleomagnetic and anisotropy of magnetic susceptibility study. Tectonics, 33(12), 2526-2551.

Pointon, M., Chew, D., Ovtcharova, M., Sevastopulo, G., Delcambre, B., 2014. High-precision U–Pb zircon CA-ID-TIMS dates from western European late Viséan bentonites. J. Geol. Soc. Lond., 171, pp. 649-658.

Rapp, R.P., Laporte, D., Martin, H., Shimizu, N. 2006. Experimental insights into slab–mantle interactions in subduction zones: Melting of adakite-metasomatized peridotite and the origin of the “arc signature”, Geochimica et Cosmochimica Acta, Volume 70, Issue 18, Supplement, 2006, Page A517, ISSN 0016-7037,

Rickwood, P. C. (1989). Boundary lines within petrologic diagrams which use oxides of major and minor elements. lithos, 22(4), 247-263.

Salazar, E.; Duhart, P.; Opazo, E.; Velásquez, R.; Peña, M.; Poblete, F.; Tapia, F. 2021. Avances en la geología de la parte centro-norte de isla Navarino (55°S), entre Dientes de Navarino y Puerto Williams, región de Magallanes y de la Antártica Chilena. Servicio Nacional de Geología y Minería, Informe Registrado IR-21-95: 86 p. Santiago.

Scarrow, J., Leat, P., Wareham, C.D., Millar, I., 1998. Geochemistry of mafic dykes in the Antarctic Peninsula continental-margin batholith: a record of arc evolution. Contrib. Mineral. Petrol. 289–305.

Sernageomin (2003) Mapa Geológico de Chile: versión digital, escala 1:1,000,000. Servicio Nacional de Geología y Minería, Santiago, Chile

Slama, J., Košler, J., Condon, D.J., Crowley, J.L., Gerdes, A., Hanchar, J.M., Horstwood, M.S.A., Morris, G.A., Nasdala, L., Norberg, N., Schaltegger, U., Schoene, B., Tubrett, M.N., Whitehouse, M.J., 2008. Plešovice zircon — a new natural reference material for U–Pb and Hf isotopic microanalysis. Chemical Geology 249 (1–2), 1–35.

Suárez, M., 1977. Notas geoquimicas preliminares del Batolito Patagonico al sur de Tierra del Fuego. Chile. Rev.geol. Chile 4, 15–33.

Suárez, M. 1978. Geología de la región al sur del Canal Beagle, Instituto de Investigaciones Geológicas, Carta Geológica de Chile, N°46, 48 p.

Suárez, M.; Hervé, M.: Puig, A. 1987. Cretaceous diapiric plutonism in the southern Cordillera, Chile. Geological Magazine, 124(06), 569. doi:10.1017/s0016756800017398

Suárez, M.; Hervé, M.; Puig, A. 1982. El Complejo Plutónico Santa Rosa, Isla Navarino: Emplazamiento sin tectónico (y/o diapirico). III Congreso Geológico Chileno, Concepción-Chile.

Suárez, M.; Hervé, M.; Puig, A. 1985. Hoja Isla Hoste e Islas Adyacentes. Servicio Nacional de Geología y Minería, Carta Geológica de Chile 65: 113 p., 1 mapa a escala 1:250.000.

Suárez, M; Pettigrew, T.H. 1976. An Upper Mesozoic island arc back-arc system in the southern Andes and South Georgia. Geol. Mag., Vol. 113, No. 4, p. 305-328.

Sun, S.S., McDonough, W.F., 1989. Chemical and isotopic systematics of oceanic basalts: implications for mantle composition and processes. In: Saunders, A.D., Norry, M.J. (Eds.), Magmatism in Ocean Basins. Geologogical Society of London Special Publication 42, pp. 313–345.

Steiger, R.H. and Jager, E. (1977) Subcommision on geochronology: Convention on the use of decay constants in geo and cosmochronology. Earth Planetary Science Letters, 36, 359-362. doi:10.1016/0012-821X(77)90060-7

Stern, C. 1980. Geochemistry of Chilean ophiolites, evidence for the compositional evolution of the mantle source of back-arc basin basalts. J Geophys Res 85(B2):955–966

Stern C.; Mohseni P.; Fuenzalida R. 1991. Petrochemistry and tectonic significance of Lower Cretaceous Barros Arana Formation basalts, Southernmost Chilean Andes. J S Am Earth Sci 4:331–342

Stern C., De Wit M. 2003. Rocas Verdes ophiolites, Southernmost South America: remnants of progressive stages of development on oceanic-type crust in a continental margin back-arc basin. In Dilek Y, Robinson PT (eds) Ophiolites in earth history. Geol Soc Spec Publ 218:1–19

Stern, C.R., Kilian, R., 1996. Role of the subducted slab, mantle wedge and continental crust in the generation of adakites from the Andean Austral Volcanic Zone. Contributions to Mineralogy and Petrology 123, 263e281.

Rapalini, A. E., Bettucci, L. S., Badgen, E., & Vásquez, C. A. (2015). Paleomagnetic study on mid-Paleoproterozoic rocks from the Rio de la Plata craton: Implications for Atlantica. Gondwana Research, 27(4), 1534-1549.

Rickwood PC (1989) Boundary lines between petrologic diagrams which use oxides of major and minor elements. Lithos 22:247–263

Taylor, S.R., McLennan, S.M., 1995. The geochemical evolution of the continental crust. Rev. Geophys. 33, 241–265.

Torres Carbonell, P.; Cao, S., González Guillot, M., Mosqueira, V., Dimieri, L., Duval, F., Scaillet, S. The Fuegian thrust-fold belt: From arc-continent collision to thrust-related deformation in the southernmost Andes, Journal of South American Earth Sciences, Volume 102, 2020, 102678, ISSN 0895-9811, https://doi.org/10.1016/j.jsames.2020.102678.

Torres Carbonell, P.J., Dimieri, L.V., Olivero, E.B., Bohoyo, F., Galindo-Zaldivar, J., 2014. Structure and tectonic evolution of the fuegian Andes (southernmost south America) in the framework of the scotia arc development. Global Planet. Change 123, Part B, 174‑188.

Torres García, M.F., Calderón, M., Ramírez de Arellano, C., Hervé, F., Opitz, J., Theye, T., Fanning, C.M., Pankhurst, R., González-Guillot, M., Fuentes, F., Babinski, M. Trace element composition of amphibole and petrogenesis of hornblendites and plutonic suites of Cretaceous magmatic arcs developed in the Fuegian Andes, southernmost South America, Lithos, Volumes 372–373, 2020, 105656, ISSN 0024-4937, https://doi.org/10.1016/j.lithos.2020.105656.

Ulianov, A., Muntener, O., Schaltegger, U., Bussy, F., 2012. The data treatment dependant variability of U–Pb zircon ages obtained using mono-collector, sector field, laser ablation ICP-MS. J. Anal. At. Spectrom. 27, 663–676.

Vermeesch, P. (2018). IsoplotR: A free and open toolbox for geochronology. Geoscience Frontiers, 9(5), 1479-1493.

Villar, L., Acevedo, R. y Lagorio, S. 2007. The Puente Quemado gabbro, to the west of Ushuaia, Tierra del Fuego, Argentina. International Congress on the Geology and Geophysics of the Southern Hemisphere (GeoSur), Actas 1: 172, Santiago de Chile.

Watters, W. 1965. Prehnitization in the Yahgan formation of Navarino island, southernmost Chile. Mineralogical magazine and journal of the Mineralogical Society, 34(268), 517-527.

Whalen, J., Hildebrand, S. Trace element discrimination of arc, slab failure, and A-type granitic rocks, Lithos, Volumes 348–349, 2019, 105179, ISSN 0024-4937, https://doi.org/10.1016/j.lithos.2019.105179.

Wiedenbeck, M., Alle, P., Corfu, F., Griffin, W.L., Meier, M., Oberli, F., von Quadt, A., Roddick, J.C., Spiegel, W., 1995. 3 natural zircon standards for U-Th-Pb, Lu-Hf, trace element and REE analyses. Geostand. Newslett. 19, 1–23.

Zen, E., 1988. Phase relations of peraluminous granitic rocks and their petrogenetic implications. Annu. Rev. Earth Planet. Sci. 16, 21–51.

Fig 1. Geological map of the main units exposed in the southernmost Andes of South America (modified after Suárez et al. 1985, Olivero and Martinioni, 2001; SERNAGEOMIN, 2003). Black circle in Tierra del Fuego represents the approximate location of the Gabbro Puente Quemado unit. Box show location of Figure 2. BCFZ: Beagle Channel Fault Zone; MFFZ: Magallanes Fagnano Fault Zone.

Fig 2. Geological map of northwestern Navarino Island and surrounding regions compiled from Suárez et al. (1985), González Guillot et al., (2018), Salazar et al. (2021) and this work.

Fig.3. Dientes de Navarino Microdioritic Sills (DNMS). (a,b,c) General view of sills intruding the Yahgán Formation (Lower Cretaceous). (d) Porphyritic texture at a hand-specimen scale, where amphibole and pyroxene phenocrysts are slightly aligned. (e) Photomicrograph with porphyritic texture with plagioclase phenocrysts within a groundmass composed of clinopyroxene and plagioclase. Cpx: clinopyroxene; Pl: plagioclase. Crossed polars, scale bar is 500 µm.

Fig.4. Castores Plutonic Complex exposed near the Estancia Santa Rosa locality. (a) Hornblende-biotite bearing tonalites host highly elongated microgranular mafic enclaves (enclave swarm). (b) Magmatic layering in diorites and tonalites cutt by small fractures (c) Gabbro bodies cut by tonalitic veins, note the pegmatitic amphiboles at the contact zone.

Fig.5. Petrography of the hornblende-bearing rocks of the Castores Plutonic Complex. (a, b) Foliated hornblende-bearing diorites with oriented tabular minerals (plagioclase and amphibole). (c, d) Metatonalites with proto-mylonitic fabrics (plagioclase and amphibole crystals surrounded by a proto-mylonitic matrix) with deformation twinning (polysynthetic and albite twins). (e) Amphibole, magnetite and apatite inclusions in a plagioclase crystal in a leucocratic tonalite. (f) Coarse amphibole gabbro with altered plagioclase (sericite). Amp: amphibole; Pl: plagioclase. All photomicrographs are under crossed polars, except (a).

Fig.6. Samantha Monzonites. (a) Post-tectonic pluton cutting the Alenghi fault generating reddish alteration in Yahgán Formation and Dientes de Navarino Microdioritic Sills (DNMS). (b) Pluton intruding the Yahgán Formation and forming orange-coloured hydrothermal alteration. (c) White metric-scale dyke (dashed yellow line) associated with the Samantha Monzonites apophyses intruding Yahgán Formation.

Fig. 7. Samantha Monzonites photomicrographs: (a to d) Pyroxene-biotite bearing quartz-monzonite. (e-f) Hornblende quartz-monzodiorite. Kfs: potassium feldspar; Cpx: clinopyroxene; Amp: amphibole; Pl: plagioclase; Mt: magnetite; Qz: quartz (plane-polarised light on the left-hand panels; cross-polarised light on the panels to the right).

Fig.8. Geochemical data from the intrusive rocks of Navarino Island and nearby localities. (a) Multi-cation discrimination plot from de La Roche et al. (1980). (b) FeO number versus wt% SiO_2, showing the boundary between ferroan and magnesian plutons, and fields of Mesozoic Cordilleran I-type, A- and S-type as defined by rocks in the Lachlan Fold Belt (Frost et al., 2001; Landenberg and Collins. 1996). (c) K_2O versus SiO_2 diagram after Rickwood (1989). (d) Modified alkali-lime index of Peacock (1931) showing the fields of the alkalic, alkali calcic, calc-alkaline, and calcic series. (e) Na_2O versus K_2O diagram with the fields of I- and S-type rocks (boundary line between the two types of granites is from Chappell and White (1974)). (f) Aluminium saturation index (ASI) plot of Maniar and Piccoli (1989), (Al/Na+K) and (Al/Ca+Na+K) are defined as molecular ratios and take into account the presence of apatite so that rocks with ASI N 1.0 are corundum-normative and are termed peraluminous (Zen, 1988). (g) Discrimination diagram between adakite vs normal arc rocks (Drummond and Defant, 1990). (h) Rb vs Yb + Nb

discrimination diagram for tectonic settings from Pearce et al. (1984). WPG: within plate granites, VAG: volcanic arc granites, ORG: ocean ridge granites, syn-COLG: syn-collisional granites. (i) La/Yb versus Nb/Y diagram with northern-central AVZ Austral Volcanic Zone pattern (dashed red line, Stern and Kilian, 1996) and normal arc rocks, i.e. melts from peridotite hybridized by aqueous fluids (dashed black lines, modified from Martin et al., 2010). Data from the Ushuaia Pluton (González Guillot et al., 2018), Ushuaia Peninsula Andesites (González Guillot et al., 2010), Puente Quemado Gabbro (González Guillot et al., 2016) and plutons of Fuegian Batholith (Montes, 2013) are also presented.

Fig.9. Diagrams showing La_n/Yb_n, SiO_2, Sr/Y and Eu/Eu versus the age of the intrusive rocks of Navarino Island. They are complemented with data from the Ushuaia Pluton (González Guillot et al., 2018), Ushuaia Peninsula Andesites (UPA) (González Guillot et al., 2010) and some plutons with ages of ~ 96-67 Ma from the Fuegian Batholith (Montes, 2013).*

Fig.10. Rare earth element and trace element abundances of the intrusive rocks from Navarino Island (the left-handed panel) and neighbouring relevant intrusive units (the right-handed panel). (a,b) Normalised to the N-MORB values of Sun and McDonough (1989). (c,d) Same units normalised to the Upper Continental Crust values of Taylor and McLennan (1995). They are complemented with data from the Ushuaia Pluton (González Guillot et al., 2018), Ushuaia Peninsula Andesites (González Guillot et al., 2010) and some plutons of Fuegian Batholith (Montes, 2013). The SiO_2 contents for each group are given in parentheses.

Fig 11. $^{40}Ar/^{39}Ar$ age spectra of intrusive rocks on Navarino Island. (a) Sample INV-05d, a hornblende microdiorite from a Dientes de Navarino Microdioritic Sill. (b) Sample INS-23d, a hornblende microdiorite from a Dientes de Navarino Microdioritic Sill. (c) Sample INV-10d, a pyroxene-biotite bearing quartz-monzonite of the Samantha Monzonites. (d) Sample INS-10d, a hornblende bearing quartz-monzodiorite of the Samantha Monzonites. Plateaus are defined according to Dalrymple and Lanphere (1974). All uncertainties are ±2σ.

Fig 12. Zircon U-Pb LA-ICP-MS geochronological data. Wetherill concordia plots are on the left-hand panels and weighted mean $^{206}Pb/^{238}U$ age are on the right-hand panels where the bars represent single ablation spots with an uncertainty of 2σ. (a-b) sample INS-57d. (c-d) sample INS-45d. (e-f) sample INS-10d.

Fig 13. Chronostratigraphic chart listing the main intrusive pulses/units and deformation events seen in distinct geographical domains in southern South America.

Fig 14. Schematic diagrams of the tectono-magmatic evolution of the Tierra del Fuego region with emphasis on the main magmatic suites from Navarino Island and Ushuaia emplaced during Cretaceous – Early Paleocene. a) Opening of Rocas Verdes basin associated with rifting, deposition of the siliciclastic Yahgán Formation with coeval volcanism and seafloor spreading; b) Early stages of Rocas Verdes basin closure and emplacement of the pre-tectonic Dientes de Navarino Microdioritic Sills; c) Arc-Continent collision, uplift, obduction of the Tortuga Ophiolite and emplacement of the Castores Plutonic Complex (also Beagle Suite and Ushuaia Peninsula Andesites); d) Slab flattening event and generation of rear-arc shoshonitic magmatism in Argentinian Tierra del Fuego; Fuegian Potassic Magmatism (i.e, Ushuaia Pluton and other plutons as discussed in the main text); e) increase in the subduction angle lead to a trench-ward arc migration as recorded by the Samantha Monzonites and the Seno Año Nuevo suite to the south. Sources: Stern et al. (1991), Klepeis et al. (2010), Torres Carbonell et al. (2014), González-Guillot (2016), Torres Carbonell et al. (2020).

Figure 1

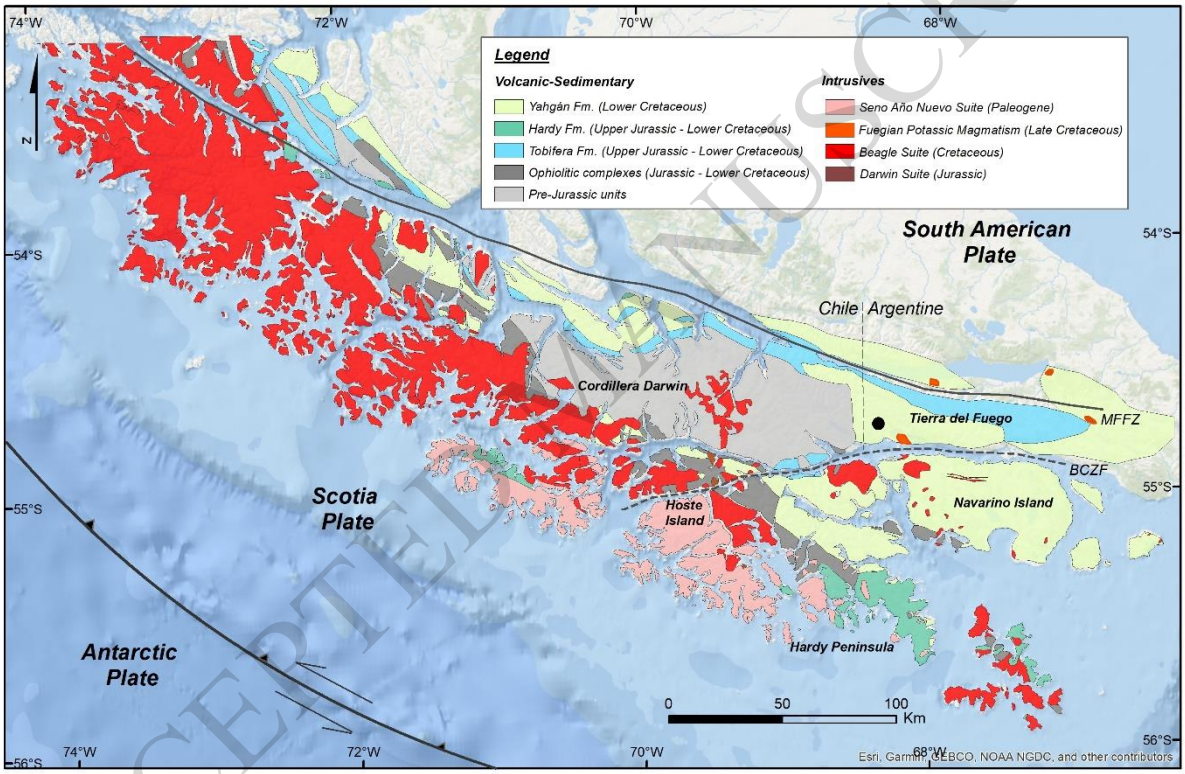

Figure 2

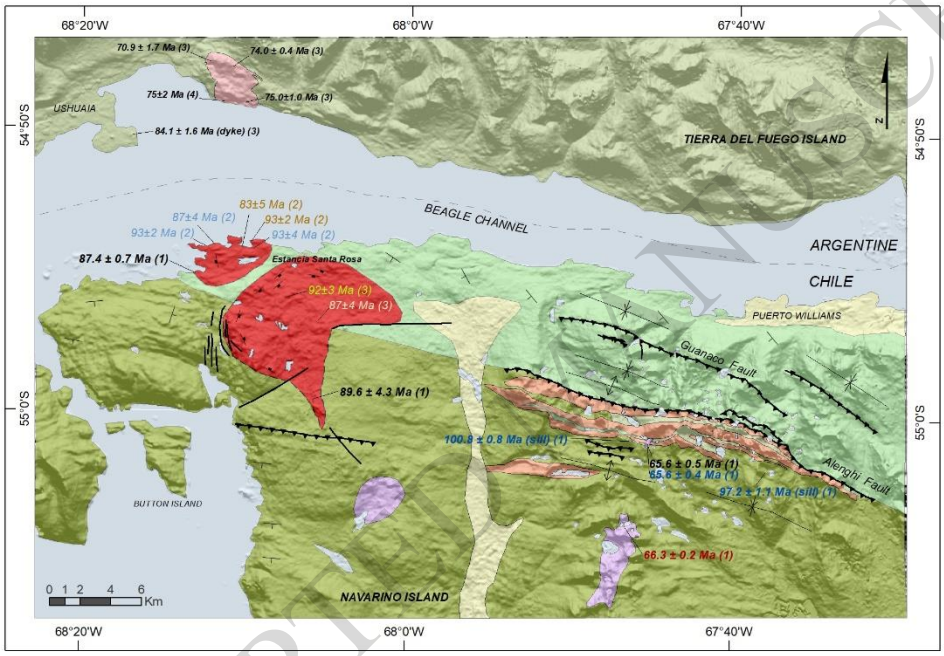

Intrusive units

- *Samantha Monzonites (66-65 Ma)*
- *Ushuaia Pluton (75-70 Ma)*
- *Castores Plutonic Complex (90-87 Ma)*
- *Dientes de Navarino Microdioritic Sills (101-97 Ma)*

Sedimentary units

- *Quaternary deposits*
- *Yahgán Fm. / Onashaga Member (Lower Cretaceous)*
- *Yahgán Fm. / Laguna Hermosa Member (Lower Cretaceous)*
- *Yahgán Fm. / undifferentiated (Lower Cretaceous)*

Simbology

- *Reverse fault*
- *Indeterminated fault*
- *Anticline*
- *Sincline*
- *Bedding dip and strike*
- *Magmatic foliation*

Geochronological data

Method / Mineral

- ***U-Pb zircon***
- ***Ar-Ar biotite***
- ***Ar-Ar hornblende***
- *K-Ar biotite*
- *K-Ar hornblende*
- *K-Ar plagioclase*

References

(1) This work
(2) Suárez et al. (1985)
(3) González Guillot et al. (2018)
(4) Barbeau et al. (2009)

Figure 3

Figure 4

Figure 5

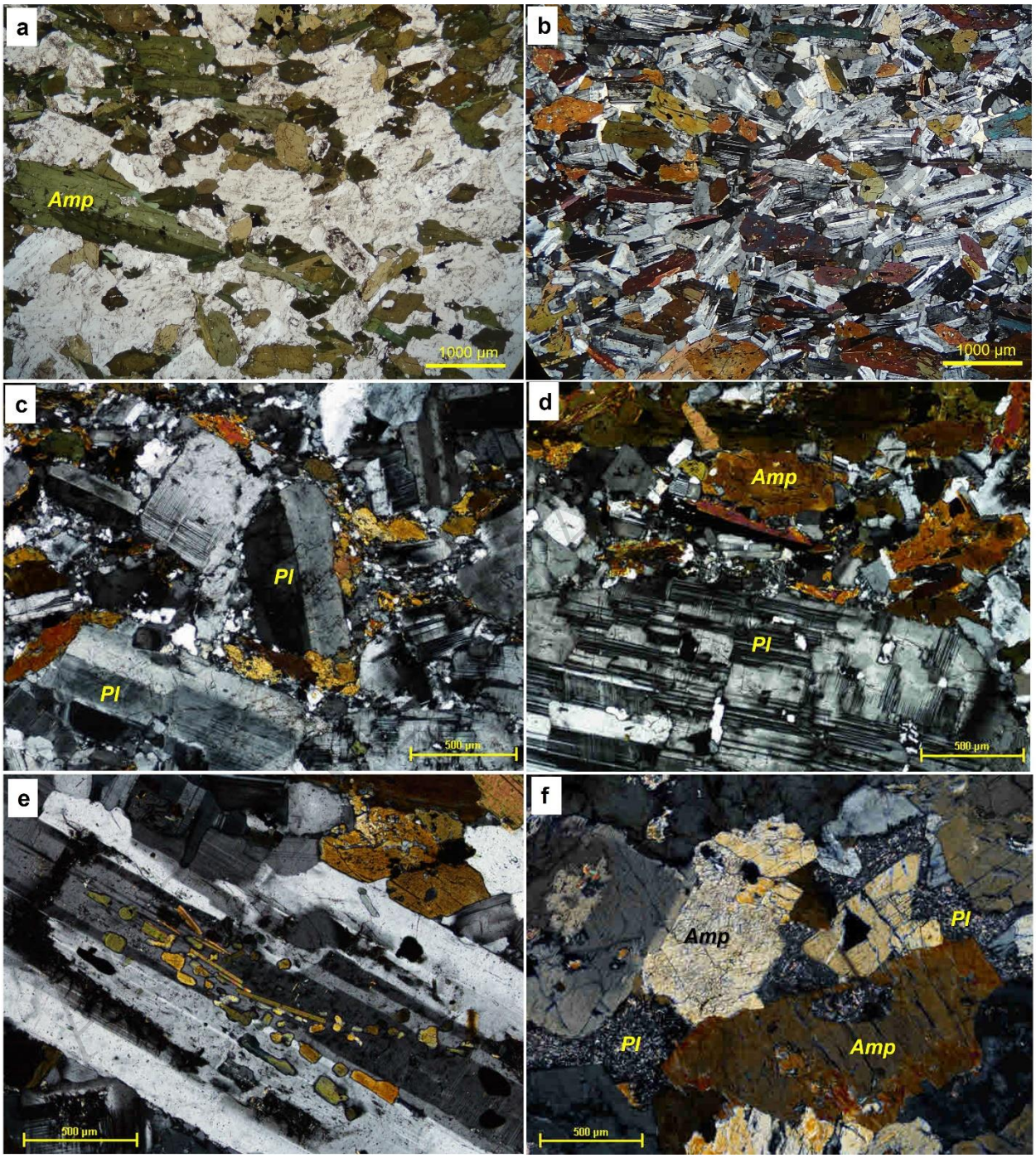

Figure 6

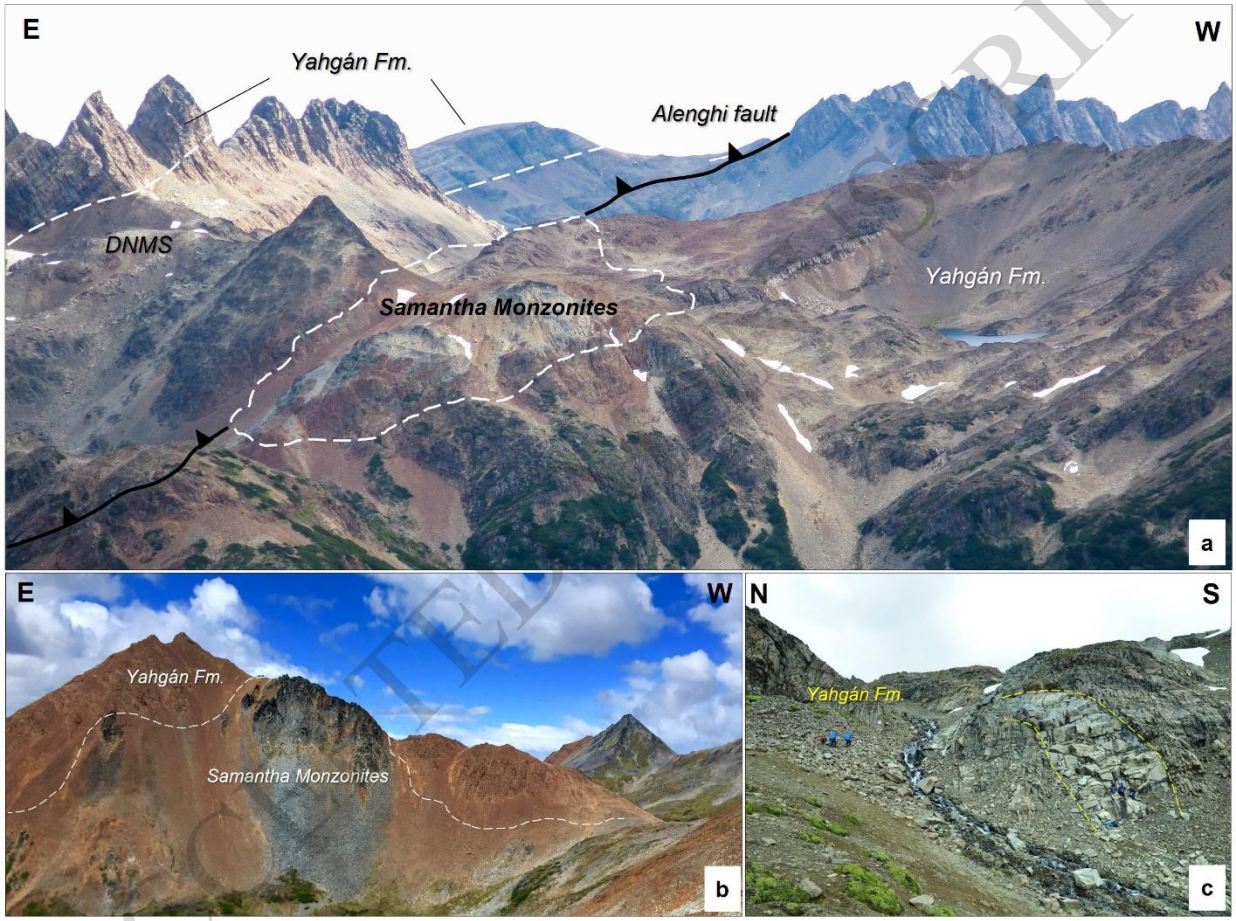

Figure 7

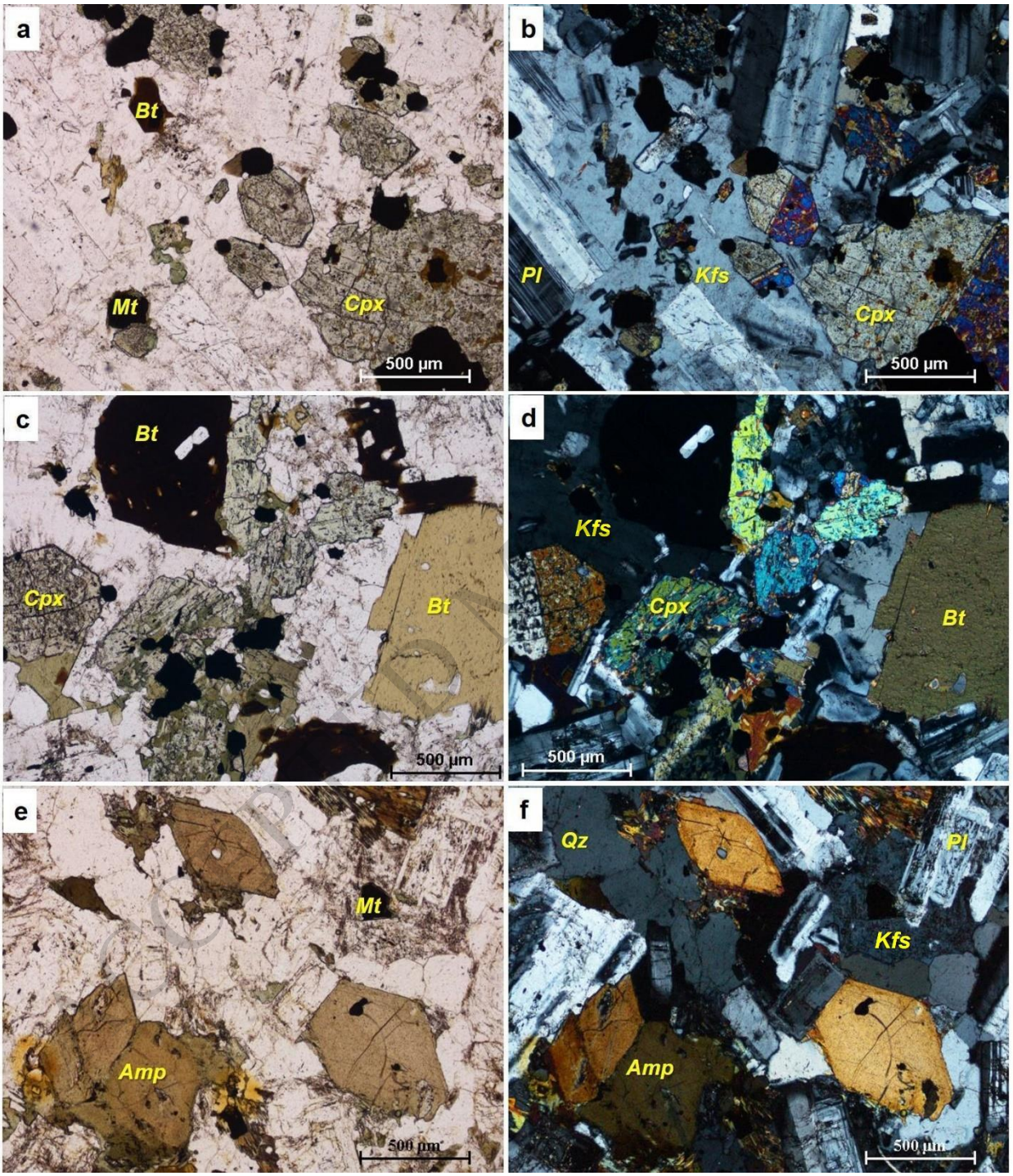

Figure 8

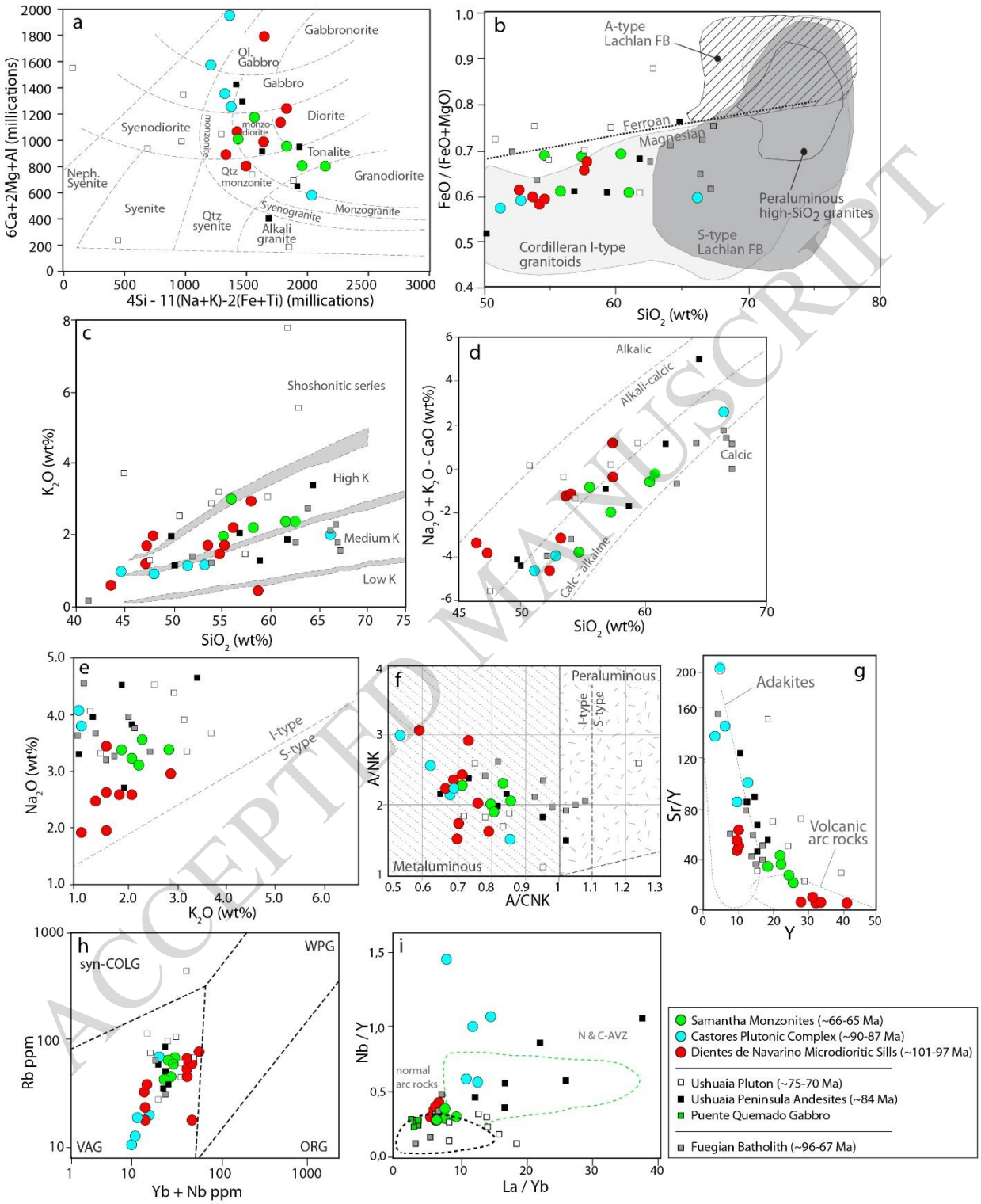

Figure 9

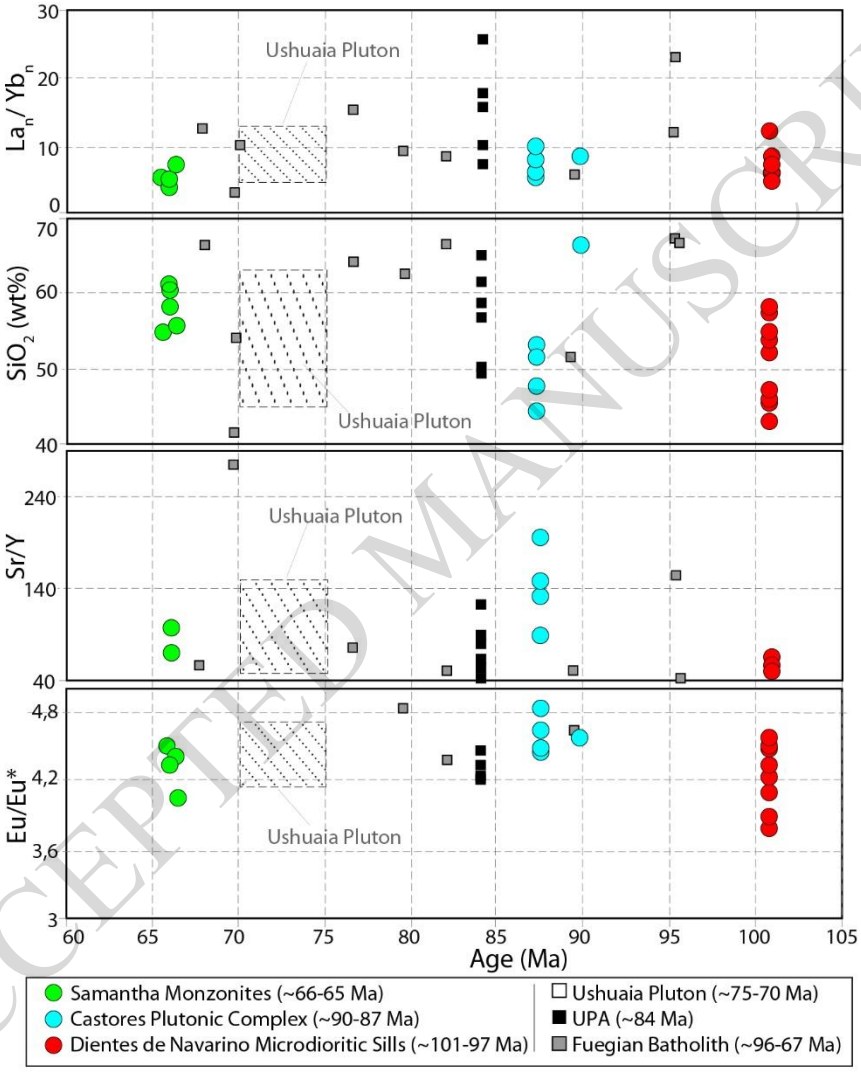

Figure 10

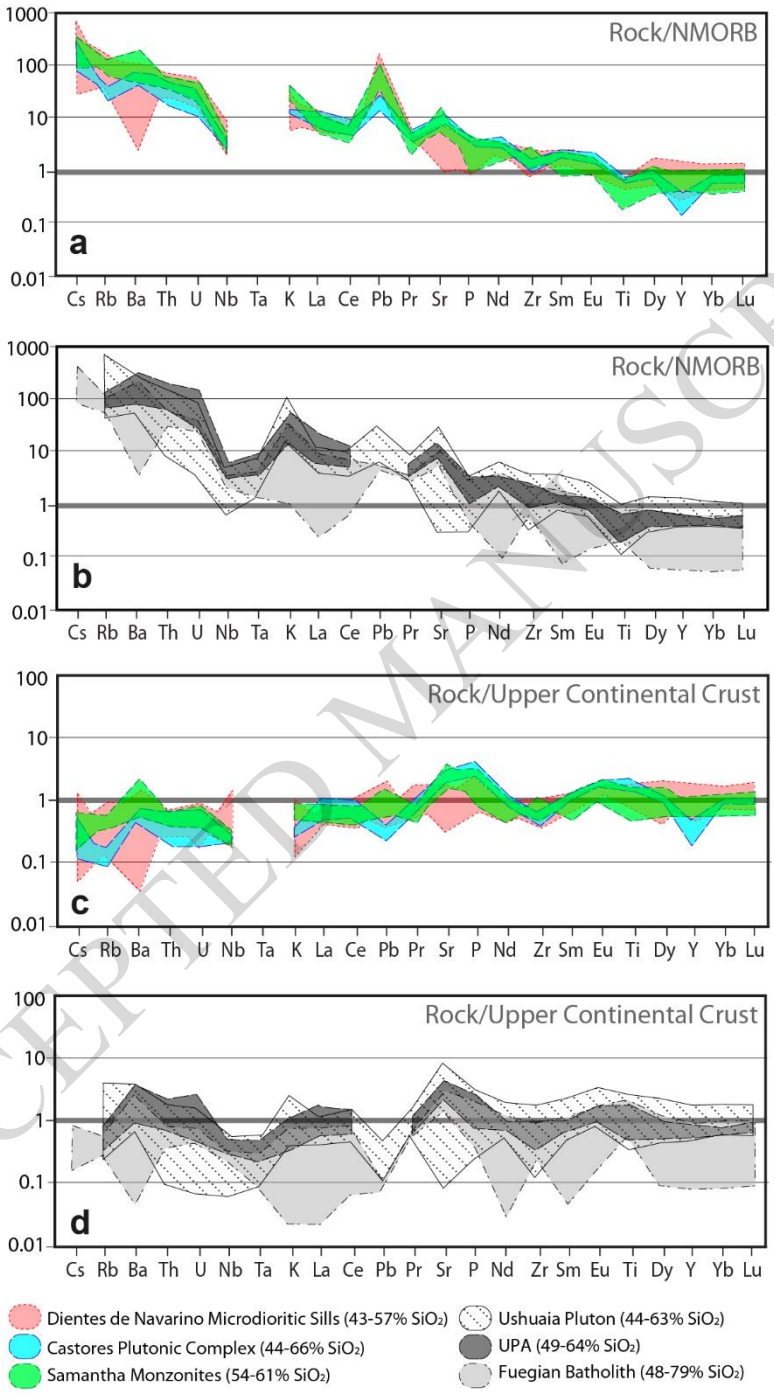

Figure 11

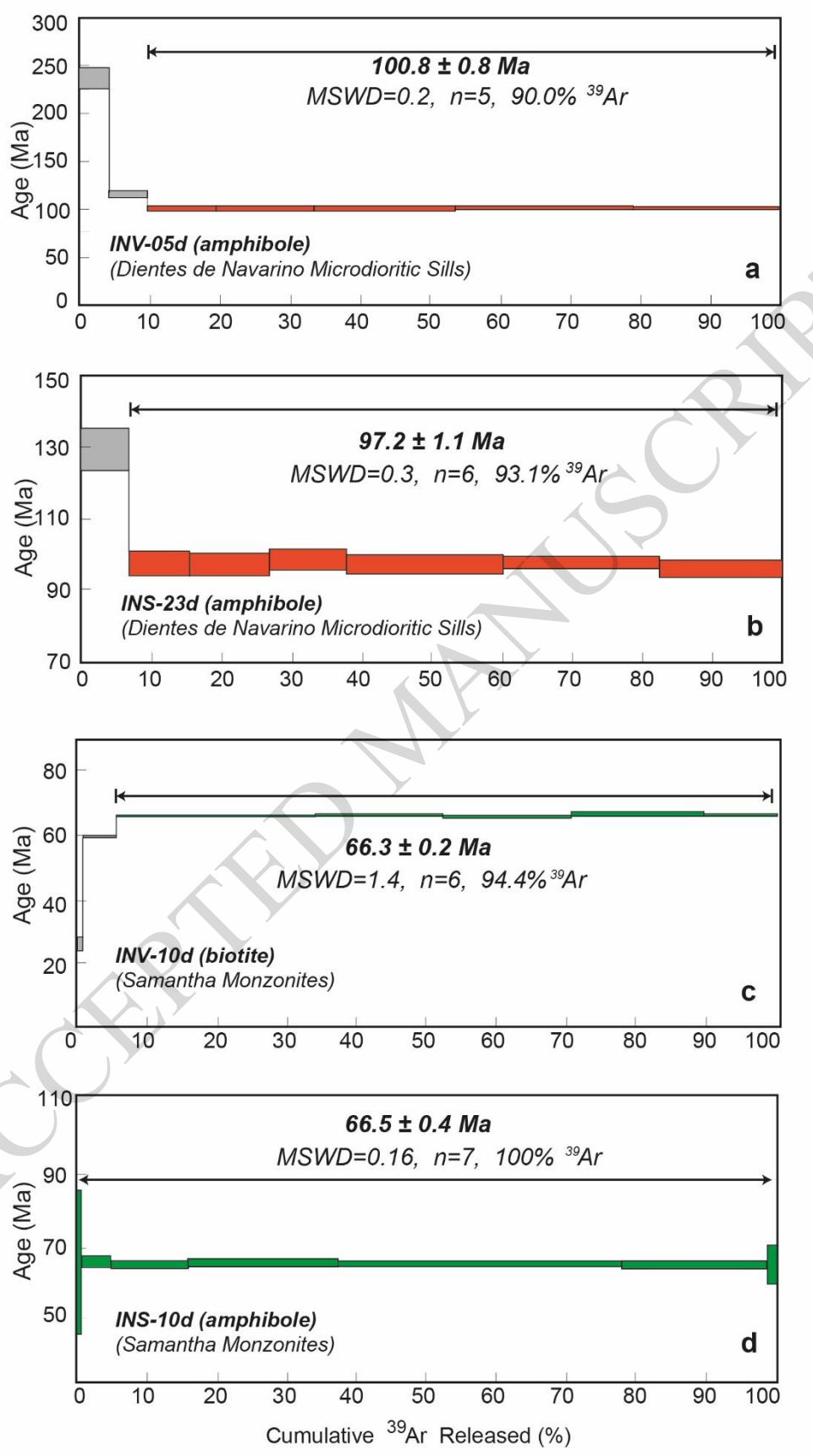

Figure 12

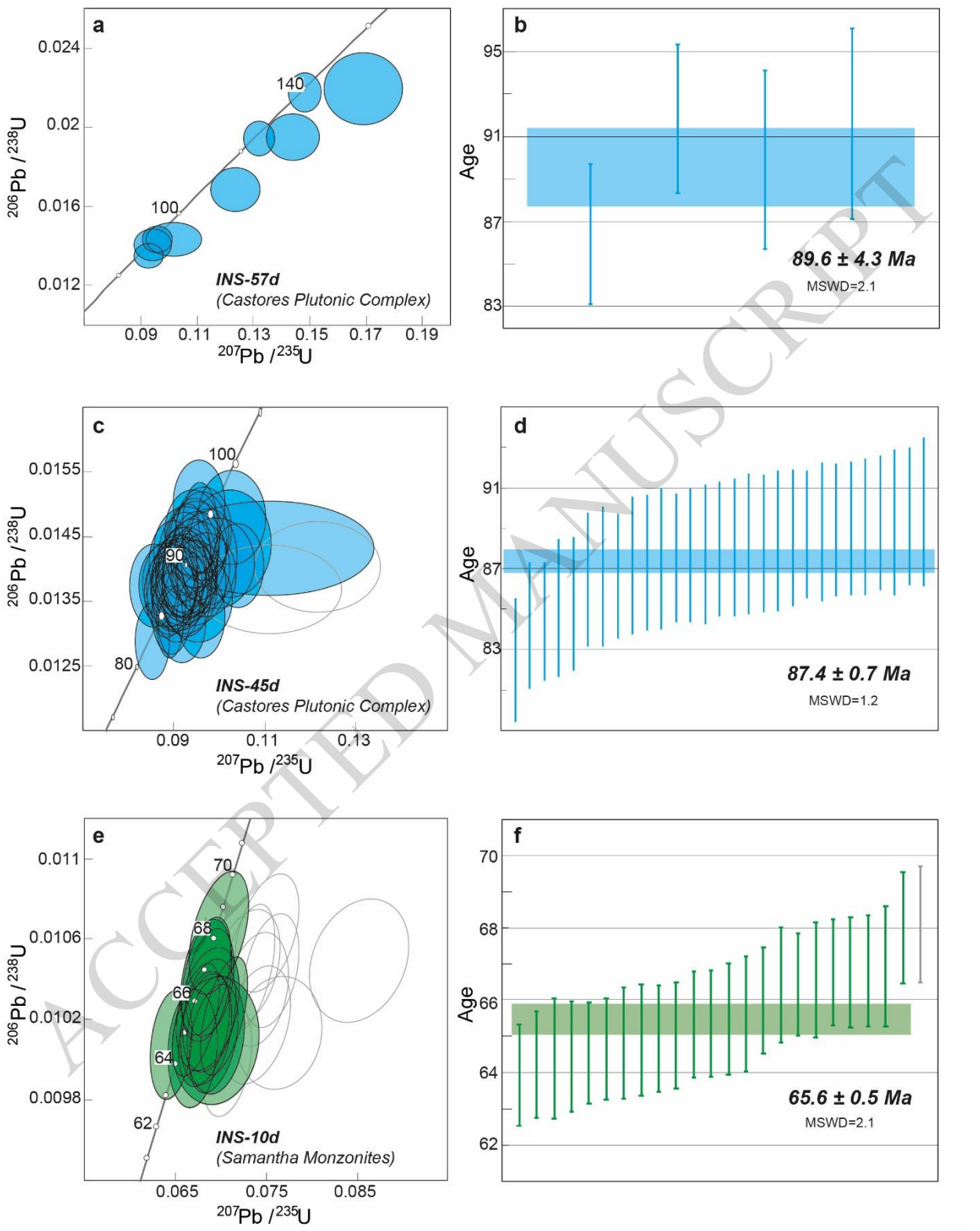

Figure 13

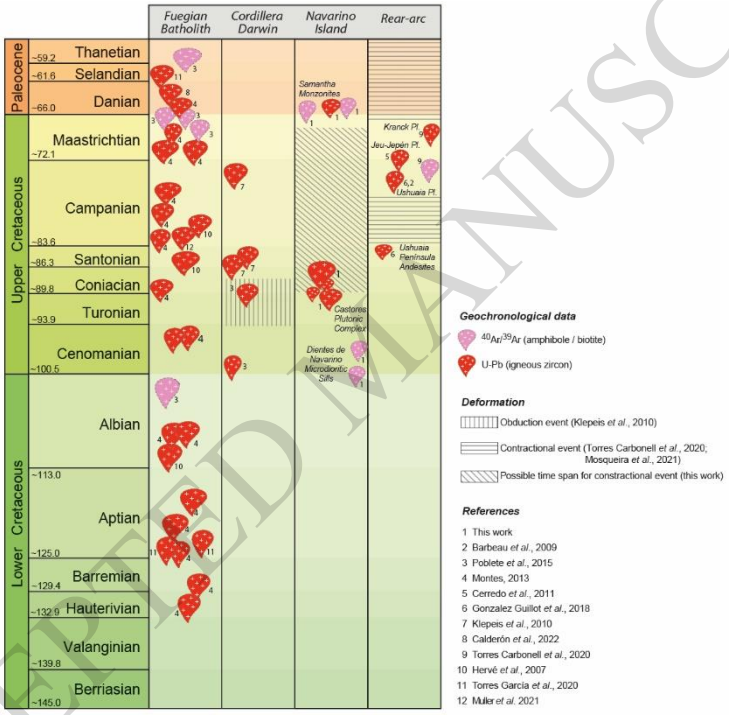

Figure 14

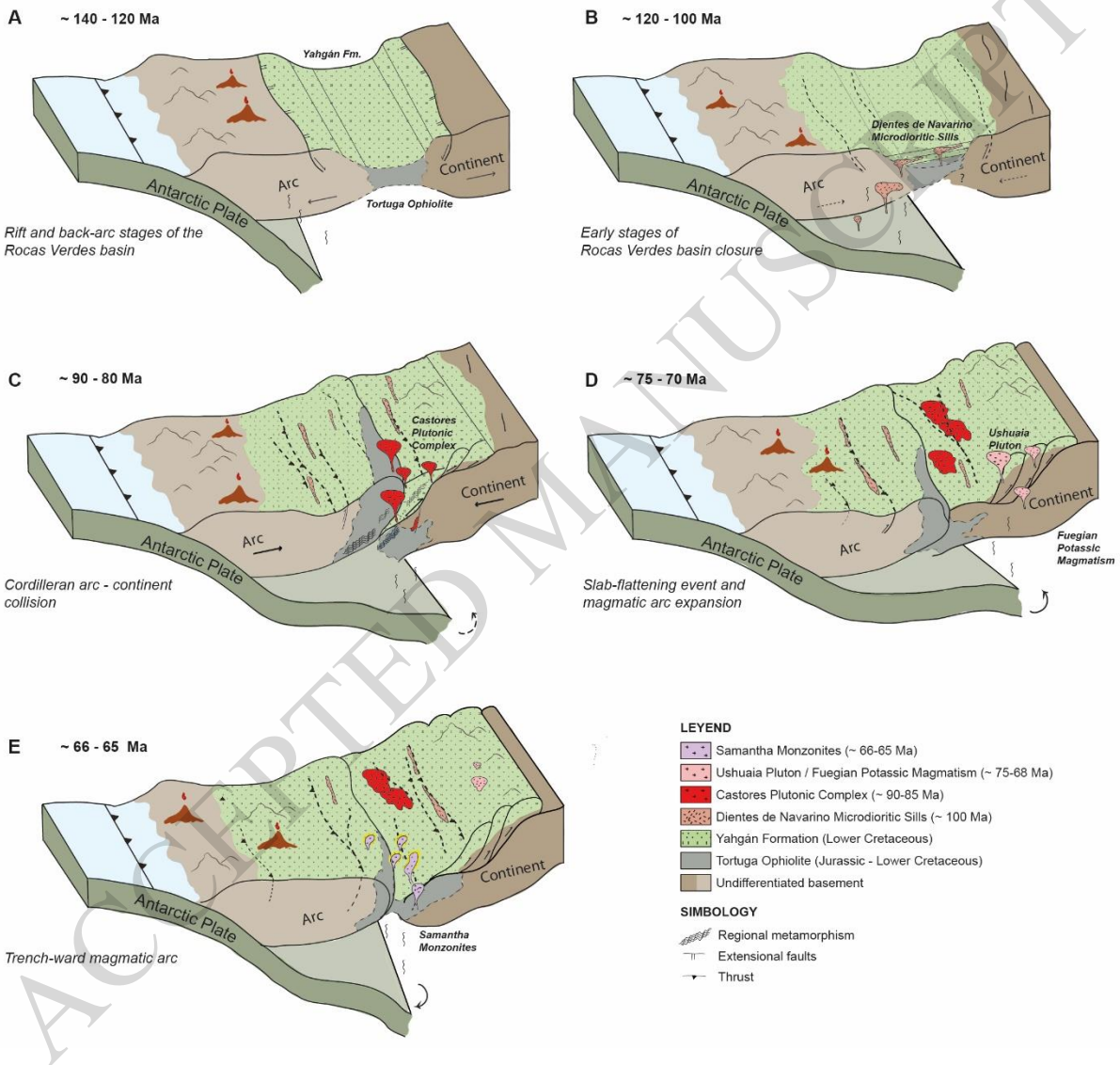

Table 1

Geochronological data for intrusive rocks of Navarino Island

Sample	UTM Coordinates	Geological unit	Lithology	Mineral	Age (Ma)	Method	Study
INV-05d	**578990 E / 3902787 N**	**Dientes de Navarino microdioriic sills**	**Hbl microdiorite**	**Hornblende**	**100.8±0.8**	**^{40}Ar/^{39}Ar**	**This work**
INS-23d	**586936 E / 3901035 N**	**Dientes de Navarino microdioriic sills**	**Hbl microdiorite**	**Hornblende**	**97.2±1.1**	**^{40}Ar/^{39}Ar**	**This work**
SR-33D	552628 E / 3914880 N	Castores Plutonic Complex	Granodiorite (dyke)	Biotite	93±2	K-Ar	Suárez et al. (1985)
SR-107	550273 E / 3913514 N	Castores Plutonic Complex	Granodiorite	Hornblende	92±3	K-Ar	Suárez et al. (1985)
INS-57d	**557681 E / 3906246 N**	**Castores Plutonic Complex**	**Tonalite**	**Zircon**	**89.6±4.3**	**U-Pb**	**This work**
SR-1	No information	Castores Plutonic Complex	Hbl Melanogabbro	Hornblende	89±7	K-Ar	Suárez et al. (1987)
IN-5-3	555898 E / 3911752 N	Castores Plutonic Complex	Granodiorite	Biotite	89±2	K-Ar	Suárez et al. (1985)
SR-107	No information	Castores Plutonic Complex	Granodiorite	Hornblende	88±6	K-Ar	Suárez et al. (1987)
INS-45d	**550195 E / 3913955 N**	**Castores Plutonic Complex**	**Foliated diorite**	**Zircon**	**87.4±0.7**	**U-Pb**	**This work**
SR-61	No information	Castores Plutonic Complex	Quartz-monzodiorite	Hornblende	86±5	K-Ar	Suárez et al. (1987)
IN-26	No information	Castores Plutonic Complex	Diorite	Hornblende	84±6	K-Ar	Suárez et al. (1987)
IN-13-2	No information	Castores Plutonic Complex	Diorite (dyke)	Hornblende	84±5	K-Ar	Suárez et al. (1987)
H-142	No information	Canal Beagle Plutonic Group	Tonalite	Biotite	84±2	K-Ar	Suárez et al. (1985)
H-64-13	553576 E / 3914483 N	Castores Plutonic Complex	Diorite	Hornblende	83±5	Rb-Sr	Halpern y Rex (1972)
SR-33C	No information	Castores Plutonic Complex	Quartz-diorite	Hornblende	82±7	K-Ar	Suárez et al. (1987)
SR-164	550273 E / 3913514 N	Castores Plutonic Complex	Quartz-monzodiorite	Hornblende	82±4	K-Ar	Suárez et al. (1987)
SR-110	No information	Castores Plutonic Complex	Granodiorite	Hornblende	81±6	K-Ar	Suárez et al. (1987)
H-64-8	553576 E / 3914483 N	Castores Plutonic Complex	Diorite	Biotite	81±5	Rb-Sr	Halpern y Rex (1972)
INV-10d	**578108 E / 3897458 N**	**Samantha Monzonites**	**Px-bt quartz-monzonite**	**Biotite**	**66.3±0.2**	**^{40}Ar/^{39}Ar**	**This work**
INS-10d	**579857 E / 3902893 N**	**Samantha Monzonites**	**Hbl qz-monzodiorite**	**Zircon**	**65.6±0.5**	**U-Pb**	**This work**
INS-10d	**579857 E / 3902893 N**	**Samantha Monzonites**	**Hbl qz-monzodiorite**	**Hornblende**	**65.6±0.4**	**^{40}Ar/^{39}Ar**	**This work**